

# UC Davis

## UC Davis Electronic Theses and Dissertations

### Title

Only time will tell: leaf stress indices derived from leaf-level hyperspectral measurements in a California vineyard demonstrate diurnal sensitivity patterns

### Permalink

<https://escholarship.org/uc/item/12z3g9mx>

### Author

Daman, Nicholas

### Publication Date

2023

### Supplemental Material

<https://escholarship.org/uc/item/12z3g9mx#supplemental>

Peer reviewed|Thesis/dissertation

Only time will tell: leaf stress indices derived from leaf-level hyperspectral measurements in a California vineyard demonstrate diurnal sensitivity patterns

By

NICHOLAS DAMAN  
THESIS

Submitted in partial satisfaction of the requirements for the degree of

MASTER OF SCIENCE

in

Viticulture & Enology

in the

OFFICE OF GRADUATE STUDIES

of the

UNIVERSITY OF CALIFORNIA

DAVIS

Approved:

---

Megan Bartlett, Chair

---

Elizabeth Forrestel

---

Andrew McElrone

Committee in Charge

2023

## **Abstract**

Grape quality and yield are goals in viticultural management that are affected by numerous abiotic and biotic factors. Field heterogeneity complicates vineyard management by producing grapes with variable stress responses and ripening patterns. Manipulation of vine water stress via irrigation is a powerful management tool influencing canopy growth and berry development. To optimize water use in a changing climate, novel techniques in precision viticulture are being developed. Increasingly, growers use satellite remote sensing tools to evaluate the heterogeneity of vineyards and to help achieve viticultural targets. Hyperspectral Vegetation Indices (HVIs) facilitate comparisons of plant stress responses at the leaf, canopy, or vineyard level. We leveraged leaf-level data collected through the Grape Remote sensing Atmospheric Profile and Evapotranspiration eXperiment (GRAPEX) to evaluate linkages between grapevine water stress and spectral indices. This study takes place in an experimental vineyard near Madera, in the Central Valley of California, an area of large seasonal inputs of irrigation. The dataset includes a three-week period during which water stress was imposed. HVIs measured pre-, during, and post-water stress were collected in parallel with conventional plant stress measurements, including leaf water potential. The purpose of this experiment is to evaluate the practical use of leaf spectroscopy to monitor water status. 88 HVIs were evaluated and among these, we found that HVIs exhibited two patterns in sensitivity to water-stressed plant responses: (1) 12 HVIs detected stress earlier at 930 or 1130, while (2) 29 detected stress at 1600. This suggests that timing of satellite or other aerial overpasses, which typically occur around solar noon, and HVI(s) chosen to evaluate plant water status may be consequential in detection of plant stress.

## **Introduction**

The changing climate has resulted in unpredictable and extreme weather in California, including drought, heat waves, heat dome, and wildfires, which have severe consequences for agricultural industries in the state. California is particularly vulnerable to the impacts of climate change, since 7.9 million acres of harvested crops are irrigated and will be affected by decreased water availability (Johnson and Cody, 2015). According to a recent report, California has been experiencing severe drought conditions and water scarcity due to increasing global temperatures, which are projected to continue in the coming decades (IPCC, 2021). Current irrigation practices, especially in the San Joaquin and Central Valley, rely on unsustainable pumping of groundwater to meet irrigation demands (Mount et al., 2022).

Grape growing is one of the most significant agricultural industries in California, generating over \$6.5 billion annually (USDA-ERS, 2022). Unlike other crops, grapes are commonly grown under regulated deficit irrigation (RDI), in which vineyards receive a fraction of water lost as evapotranspiration (ET) to maintain plants at a mildly stressed status during key growing stages (Williams, 2017). This practice has been shown to improve berry quality and stimulate formation of positive sensory compounds (Bravado et al., 1985). While RDI may regulate vegetative growth, excessive stress may result in decreased yields. Stress in grapevines is conventionally monitored using measurements of stomatal conductance, soil moisture, and leaf water potential, among others (Williams et al., 2012). These tools are used widely due to simplicity of results and established thresholds for stress, especially for water potential (Ojeda, 2007; Miras-Avalos and Araujo, 2021).

A critical time in berry development is veraison, where growth accelerates, berries soften and change color, and formation of organic acids increases (Coombe, 1992). RDI prior this point

may result in smaller berries which have higher concentrations of color and flavor compounds, namely phenols and anthocyanins, largely localized in the skins (Williams and Heymann, 2017). Excessive levels of water stress may degrade anthocyanins (Afifi et al., 2021). Overall, timing and level of water stress can have a profound influence on quality and yield. Monitoring plants for stress responses is critical to inform intervention when water stress becomes too severe. However, field heterogeneity complicates the representation of plant stress at field level taken with on-the-ground measurements (e.g., leaf water potential), especially in large vineyards.

Changes in leaf reflectance result from changes in leaf chemical composition and cell structure and can be linked to plant physiological status (Tucker, 1979), structure (Hunt and Rock, 1989; Gitelson, 2003), and stress (Carter, 1994; Gitelson et al. 2001b; Zhou et al., 2021). The visible region of the electromagnetic spectrum (400-700nm), for instance, contains characteristic absorption maxima by photosynthetic pigments (Gitelson et al., 2001a, 2003). Healthy leaves reflect light differently than stressed leaves at these wavebands, which can be connected to photosynthetic efficiency (Zhou et al., 2021), alternative quenching pathways (Wong et al., 2022), or fluorescence to dissipate excess energy (Gamon et al., 1997). Other biochemistry, including lignin, nitrogen (Serrano et al. 2022), and water content (Malthus et al., 1993; Gao et al., 1996) have known wavebands at which they absorb strongly.

Plant stress responses include changes in biochemical content, which can be detected using leaf reflectance. Leaf reflectance has been well studied for several decades (Gates et al., 1965; Hunt et al., 1987; Carter, 1993; Peñuelas et al., 1993a), but recent developments in technology (e.g., artificial neural networks) have made this tool more feasible for use in observing stress in plants (Poblete et al., 2017). Leaf-level hyperspectral data gives a full understanding of leaf reflectance and may allow for a more detailed analysis of leaf composition.

However, this data collection is significantly limited spatially and temporally since measurements are manual. On the other hand, satellite or airborne images can provide data over larger areas, but the spectral resolution is usually lower (Al-Wassai and Kalyankar, 2013; Pádua et al., 2020; Tang et al., 2022). Other satellites collect data at higher spectral resolution but lower frequency. Currently, readily available satellite imagery (e.g., LANDSAT) provides low spectral and temporal resolution (Sivanpillai, 2021). In isolation, this tool is not practical for irrigation decision making, especially with unexpected weather patterns predicted over future decades. Other satellites may provide higher spectral resolution (e.g., Hypsiri; 10 nm contiguous bands from 380-2500 nm) and may soon become readily available to the public (HypsIRI Mission Concept Team , 2018).

These remote methods (e.g., satellites) as well as on-the-ground hyperspectral tools provide data which can be used to calculate hyperspectral vegetation indices (HVIs). HVIs are mathematical combinations of the reflectance values of different portions of the spectrum and have been used to monitor plant status in agricultural settings for decades (Rouse and Haas, 1974). HVIs can be formulated to be sensitive to variations in vegetation biochemistry, structure (Daughtry, 2001), pigments (Peñuelas et al., 1993a; Merzlyak et al., 1999), and water content (Malthus et al., 1993; Penuelas et al., 1997) and are widely used to measure and monitor plant growth, productivity, and stress.

Here, we evaluate a large number of HVIs leveraging the leaf-level seasonal and diurnal data acquired through the GRAPEX project. Vines were subjected to varying levels of stress, and comparisons were made between physiological measurements and hyperspectral data to determine optimal HVIs and timing for stress detection. Results are intended to inform future remote sensing applications of HVIs in plant monitoring and vineyard mapping.

## Materials and Methods

### *Study site*

The study area (RIP720) is located 25 km west of Fresno in the Central Valley of California (Figure 1). The vineyard is approximately 16 hectares, mostly sandy loam, and the climate is Mediterranean with abundant sunshine, large day-to-night temperature differences, and an average temperature between May and October of 22 °C with 12 mm of rainfall. The vineyard was planted in 2010 with Merlot (*Vitis vinifera L.*) vines trained to quadrilateral cordons on a horizontally split trellis with row spacing of 3.35 m and an inter-row distance between vines of 1.5 m in east-west row orientation. The Ripperdan vineyard is divided into four treatment blocks, each approximately 3.2 hectares in size. The period of investigation considered here is June to early August 2018.

### *Thermal-based $ET_a$ estimation*

High spatiotemporal resolution ET time series maps were generated using the Atmospheric-Land Exchange Inverse (ALEXI) surface balance model and disaggregation model (DisALEXI) with the Spatial and Temporal Adaptive Reflectance Fusion Model (STARFM) as previously described by Knipper et al. (2019). The result of this data fusion is daily 30-m resolution ET maps with a two-day latency. Weekly actual ET ( $ET_a$ ) estimates were delivered on Friday and represented a summation of daily  $ET_a$  from the prior Friday to Thursday. The last two days of the weekly ET period (Wednesday and Thursday) were estimated using the last available day model and local reference ET. A local Fresno State CIMIS Station provided grass reference ET ( $ET_{ref}$ ) values.

### *Irrigation schedule*

Irrigation at the experimental site was managed with the objective of inducing a range of stress levels within different vineyard blocks. The vineyard was divided into four blocks (treatments) as shown in Figure 1. The objective was to implement severe water stress on stressed blocks (S1 and S2) by mid-July, and then reintroduce irrigation across all blocks in order to observe recovery of stressed blocks. Irrigation decisions were made using the remote sensing model described in the previous section (Knipper et al. 2019; 2020). The first irrigation of the season was implemented the week of May 14<sup>th</sup>, with soils still at capacity from winter/spring rains. From that point, the well-watered (WW) block was irrigated according to the standard commercial practices at the site, based on a percentage of crop ET. The irrigation amounts for the other three treatments were calculated as fractions of the actual ET estimated at block level (see *Thermal-based  $ET_a$  estimation*). The objective was to induce mild water stress in the M block, and severe stress in blocks S1 and S2. Initially, the deficit over the estimated  $ET_a$  was planned as 45% in blocks S1 and S2, and 60% in the M block. However, every week, the deficits were adjusted based on observations of soil moisture and water fluxes at the site to ensure that the soils for the stressed treatments would be completely depleted close to the date when the maximum stress was planned. A hard pan at about 2 m depth exists under sections of the southern half of the vineyard (blocks M and WW), which prevented the M block from reaching the desired level of stress by the time of the field campaign (i.e., Intensive Observational Period, IOP). Even though the irrigation inputs close to the sampling were minimal (~5-10%  $ET_{ref}$ ), it took longer than expected to dry the profile. During the week of July 6-July 12, immediately preceding the “During Stress” data collection occurring on July 13<sup>th</sup>, the northern two blocks (S1 and S2) received no irrigation (0%  $ET_{ref}$ ), while the southern blocks (3 and 4) received 27% and



5.56%  $ET_{ref}$ , respectively (Figure 2). After the collection period during the water stress event, all blocks were irrigated 30-60%  $ET_{ref}$  in order to facilitate a “recovery” phase. This irrigation schedule continued during data collection on August 6<sup>th</sup>. Cumulative irrigation data for each of the blocks is shown in Figure 2.

#### *Leaf-level data*

Ground measurements were collected during three days of IOPs on June 19<sup>th</sup> (“Before Stress”), July 13<sup>th</sup> (“During Stress”), and August 6<sup>th</sup> (“After Recovery”) as a part of GRAPEX. These IOP campaigns began before dawn and measurements were taken to align with overhead satellite and unmanned aerial vehicle (UAV) passes. After the first collection time, diurnal data was collected with a 1- to 2-hour window between measurements. Collection locations are shown in Figure 1 and collection dates appear in Figure 2.

In order to capture measurements within a narrow temporal window, at least two teams were dispatched, each with the following instruments: ASD FieldSpec Hi-Res Spectroradiometer (Malvern Panalytical, Malvern, UK) with 2-nm spectral resolution and 350-2500nm spectral range, LI-6400/XT Portable Photosynthesis System (LI-COR, Lincoln, NE), Scholander-type Pressure Bomb (PMS Instruments), a hand-held infrared radiometer (IRT – Apogee Instruments Inc), a portable nitrogen tank, and foil-laminate bags. The equipment was stored on 4-wheeled “mules” to ease transport between collection points. First, the FieldSpec operator selected a fully mature leaf that was not sharing a position with a grape cluster to collect its reflectance signature using the ASD. Another person measured gas exchange parameters on the same leaf using the LI-6800. One leaf per vine was bagged using foil-laminate bags 45 minutes prior to measurement of stem water potential. Finally, the leaf was excised, and then leaf and stem water potentials were measured using the pressure bomb. Each treatment block contained three data

collection points distributed along a diagonal in the direction of predominant wind (NW). Field measurements were collected quickly, but unavoidable variability in collection times may have contributed to variation in data within and between treatment blocks.

### *Vegetation Indices (VIs)*

Leaf reflectance measurements were used to calculate Hyperspectral Vegetation Indices (HVIs) which utilize reflectance values at key wavelengths or regions of the leaf spectrum to make inferences about leaf and plant status. One common calculation is the Simple Ratio (SR), represented as the following equation:

$$SR = \frac{R_{\lambda_1}}{R_{\lambda_2}}$$

**Equation 1.** Simple Ratio (SR) calculation, where  $R_{\lambda_1}$  and  $R_{\lambda_2}$  are reflectance values at selected wavelengths.

Typically,  $\lambda_1$  is a wavelength that is sensitive to changes leaf physiology, whereas  $\lambda_2$  is often a reference wavelength. In order to restrict the range of HVI values, another common calculation is the Normalized Difference (ND), which also utilizes reflectance at two wavelengths:

$$ND = \frac{R_{\lambda_1} - R_{\lambda_2}}{R_{\lambda_1} + R_{\lambda_2}}$$

**Equation 2.** Normalized Difference (ND) calculation, where  $R_{\lambda_1}$  and  $R_{\lambda_2}$  are reflectance values at selected wavelengths.

Other calculations include waveband shifts, where selected wavelengths of published indices are shifted to nearby values based on stronger correlations to other measurements of stress. In this study, waveband shift HVIs are represented by the same name as the published

HVI followed by a number (e.g., Normalized Difference Water Index, NDWI1-6). These names were assigned based on the lowest value of the first wavelength appearing in the formula.

The HVIs that were evaluated in this study were collected from a variety of sources, including The IDB Project (Henrich et al. 2012) and reviews of HVIs (Rodríguez-Pérez et al. 2007, Roberts et al. 2011). 88 HVIs included in this evaluation are listed in Supplementary Table 1, along with their formulae. Indices were selected based on their frequency of use in scientific literature and industry (e.g., NDVI, EVI, WI) and/or to represent a diversity in wavelengths of interest in order to take advantage of the high spectral resolution data. For each of the three data collection dates, values for each HVI were calculated independently at each time of day.

### *Statistics*

HVI values for each treatment block were averaged. Significant differences between mean treatment block values at each time of day were calculated using pairwise Mann-Whitney U mean separation tests ( $\alpha=0.05$ ). The Mann-Whitney U tests were performed using the `scipy.stats` module (version 1.10.1) in Python (version 3.10.11) to calculate the test statistic and p-value. Gas exchange, leaf temperature, and leaf water potential parameters were evaluated using the same program and tests.

We used Birch (Balanced Iterative Reducing and Clustering using Hierarchies) clustering algorithm from the Scikit-learn (`sklearn.clusters`) library (version 1.2.2) in Python to perform unsupervised clustering of comparisons between evaluated HVIs and physiological parameters. This clustering model creates a clustering feature tree, which inputs data points individually and assigns values to a cluster based on their distance to the first point assessed. Specifically, we employed Birch clustering to identify groups or clusters (threshold=0.01, n=2) of similar observations in our data. Values that were grouped into clusters were assigned a binary code. To

interpret the accuracy of the model, clusters were evaluated using the Fowlkes-Mallows Index (FMI) score from the Scikit-learn (`sklearn.metrics.cluster`) library, calculated as follows:

$$FMI = \frac{TP}{\sqrt{(TP + FP) * (TP + FN)}}$$

**Equation 3.** Fowlkes-Mallows Index (FMI) score, calculating using True Positive (TP), False Positive (FP), and False Negative (FN).

FMI can be used when ground-truth labels (e.g., identity of water stress treatments) are known. FMI score measures the accuracy of cluster assignment by the Birch model based on assigned labels and actual labels of samples. The binary classification of FMI score ranges from 0 to 1, where 0 corresponds to a misclassification of all elements and 1 corresponds to a perfect classification. In this study, FMI scores closer to 1 indicate clusters are more distinct.

## Results

$ET_a$  and  $ET_a/ET_{ref}$  were nearly identical before stress was imposed (Figure 2). Data collected during the stress event on July 13<sup>th</sup> observed similarities in  $ET_a$  and  $ET_a/ET_{ref}$  between well-watered (WW and M) blocks and between stressed (S1 and S2) blocks. At this collection time, the S1 block had a slightly higher  $ET_a/ET_{ref}$  value than the S2 block. During the “After Recovery” collection period, some differences in vineyard water use and  $ET_a/ET_{ref}$  were still observed between well-watered and stressed conditions.

### *Conventional stress measures*

Several leaf physiological measurements were collected before, during, and after the water stress event that was imposed in mid-July (see seasonal trends in Figure 3). Before the stress period (measurements taken in mid-June), vines exhibited similar responses and minimal differences between blocks. In fact, blocks that were to receive stress exhibited the highest leaf

water potential ( $\Psi_{\text{leaf}}$ ) and gas exchange rates (e.g., S1 had the highest mean A and  $g_{\text{sw}}$  in the early afternoon). During the stress period,  $\Psi_{\text{leaf}}$  only became significantly different beginning at 1430 between S2 and the other blocks. At 1600 and 1700, “stressed” blocks (S1 and S2) versus “well-watered” (WW) and mildly stressed (M) blocks were significantly different. This pattern contrasts with the other three measurements (leaf temperature,  $T_{\text{leaf}}$ ; net assimilation, A; and stomatal conductance,  $g_{\text{sw}}$ ), which were sensitive to differences between stressed and well-watered blocks earlier in the day at 800 or 930. A and  $g_{\text{sw}}$  for stressed blocks were consistently lower than that of well-watered blocks. For both of these measures, at 1300, differences between blocks became smaller and by 1600 the M block was not significantly different from stressed blocks. At 1430, however, well-watered blocks were both significantly different than stressed blocks.

These measurements were also collected near a recovery phase in early August, in which all blocks were irrigated according to local commercial practices. Despite aiming for similar recovery in all blocks, at the time of data collection there were still differences in  $ET_a$  and  $ET_a/ET_{\text{ref}}$ . The previously imposed stress event showed clear carryover effects into the recovery period.  $T_{\text{leaf}}$  values for all blocks were the same until 1300. After this point, previously stressed blocks had higher  $T_{\text{leaf}}$  throughout the rest of the day in well-watered blocks. Stomatal conductance values were significantly different between stressed and well-watered at all time points, except 800, where the M block was similar to other treatments.

#### *All Hyperspectral Vegetation Indices (HVIs)*

Hyperspectral measurements taken on June 19<sup>th</sup>, July 13<sup>th</sup>, and August 6<sup>th</sup>, 2018. Differences between treatments were observed for the “Before Stress” (June 19<sup>th</sup>) and “After Recovery” periods (August 6<sup>th</sup>), which are discussed below. During the water stress period (on

July 13<sup>th</sup>), hyperspectral measurements were used to calculate HVIs (Supplementary Table 1). Of the 88 indices evaluated, 11 detected significant differences between stressed (S1 and S2) and well-watered (WW and M) blocks at 930, 12 HVIs at 1130, and 29 HVIs at 1600 “During Stress” (Supplementary Table 2). These values represent some HVIs with only slight waveband shifts of other indices. For example, NDII1 and NDII2 both utilize reflectance at 819nm, while NDII1 utilizes reflectance at 1640nm and NDII2 at 1649nm (Supplementary Figure 1). When excluding duplicate HVIs with these waveband shifts, at the collection times of 930, 1130, and 1600, there were 9, 9, and 15 unique indices, respectively. Seasonal HVI values for all 88 indices appear in Supplementary Figure 1.

HVIs demonstrated interesting sensitivity patterns, including time of day when block differences could be detected. Of the HVIs that detected significant differences between stressed versus well-watered blocks, 10 were sensitive at both 930 and 1130 (e.g., mSR1 in Supplementary Figure 2). Three HVIs detected differences between stressed versus well-watered at all three collection times (see Crt2, Crt5, and RBI in Supplementary Table 2). This contrasts with the vast majority of HVIs that were sensitive to block differences only in the morning or only afternoon collection times. A subset of these HVIs was selected to demonstrate patterns in timing of sensitivity to stress.

#### *Early separation HVIs*

Six HVIs were selected from those that were sensitive to differences between stressed versus well-watered during the morning collection times (Figure 4). These were chosen to represent indices that appear more commonly in the literature as well as to capture a diversity of waveband regions of the leaf spectrum. Prior to the imposition of water stress, selected HVIs detected some differences between blocks on June 19<sup>th</sup> (left column of Figure 4). At 1430, the S1

block had higher CAI1 values than WW block (see top left panel in Figure 4). At 1600, other selected indices detected differences between blocks (see Crt2, PSRI, and RBI panels in Figure 4). The trends observed for CAI1, Crt2, and RBI prior to imposition of stress are reversed from trends that appear during stress imposition, which corresponds with observations of conventional stress measures at this time (Figure 3).

During the water stress event, most indices that detected significant differences between stressed versus well-watered blocks at 930 also did so 1130, except CAI, which only detected these differences at 930 (Figure 4). Blocks mostly reported similar HVI values during the “after recovery” phase (right column of Figure 4). The S2 block exhibited the largest differences from the other blocks at 800 (see Crt2 and NPCI panels of Figure 4). At 1600, the M block had higher values than other blocks (see PSRI and SIPI1 of Figure 4). These responses were similarly reflected in the conventional stress measures (Figure 3).

In the afternoon, this trend is reversed, where differences between clusters is mostly due to differences in  $\Psi_{\text{leaf}}$  and not index (see right column of Supplementary Figure 2). The strongest clustering results appear in comparisons against  $g_{\text{sw}}$  (see FMI score in Supplementary Table 3). FMI scores generally decreased with time of day (see CAI1, Crt2, NPCI, and PSRI panels in Figure 5). However, FMI score for SIPI1 increased with time of day and FMI score for RBI had no relationship with time of day. Cluster comparisons between these HVIs and other remaining measures of stress ( $T_{\text{leaf}}$ , and A) appear in Supplementary Figures 4 and 5 to assure that the focal HVIs were consistently compared against conventional methods. Cluster analysis between selected HVIs and conventional measures of stress were evaluated at 930, 1130, and 1600 during the water stress period (Figure 5 and Supplementary Figures 2, 3, and 4). Birch clustering predicted groups ( $n=2$ ) that were evaluated using the Fowlkes-Mallows Index (FMI) score. FMI

assesses the accuracy and precision of the model by comparing predicted groups (from Birch model) and actual group labels (i.e., stress treatment). Comparisons between the selected HVIs and  $g_{sw}$  are included because these HVIs utilize wavelengths in the VIS and NIR regions that correspond with leaf pigments (see Table 1). Cluster analysis between early separation HVIs and  $\Psi_{leaf}$  performed poorly in the morning, where differences between clusters are mostly attributed to index values (see left and center columns of Supplementary Figure 2).

#### *Late separation HVIs*

As was the case for early separation HVIs, six HVIs were selected that demonstrated sensitivity to differences between well-watered versus stressed blocks late in the day (Figure 6). Values for the six HVIs in Figure 6 were not uniform across blocks before the water stress period. All selected HVIs detected block differences at 1430 (see left column of Figure 6). WW and S1 were different at this time in five of these HVIs. Differences between WW and S2 blocks were greatest for NDWI1. At 1600, the indices ranges are much smaller than those at earlier times of day. The M block was distinct from the other blocks for several HVIs (see MSI1, NDII1, and NDWI1 panels in Figure 6). In the CUR index, well-watered blocks had higher values than stressed blocks before the stress event.

During the imposition of water stress, four of the indices in Figure 6 also detected some block differences earlier in the day, either at 930 (see MSI1, NDII1) or 1130 (see NDWI1) or at both of these times (see WI2). MSI1, NDII1, and NDWI1 had significantly different values for WW block versus both stressed treatments in the morning, but the M block could not be separated from stressed blocks. HVI values were similar throughout the day during the “After Recovery” period (see right column of Figure 6).



Cluster analysis between selected HVIs and conventional measures of stress were evaluated at 930, 1130, and 1600 during the water stress period (Figure 7). Comparisons between the six selected HVIs and  $\Psi_{\text{leaf}}$  because these indices utilize reflectance bands in the IR and other spectral ranges where water strongly absorbs (see Table 2). FMI score was evaluated for these correlations (Supplementary Table 4). For all selected indices, FMI increased with time of day. WI2 had the highest FMI score at all times of day and at 1600, which was 1. At 930 and 1130, cluster analysis of  $g_{\text{sw}}$  and selected HVIs performed almost as well as comparisons with  $\Psi_{\text{leaf}}$  (see Supplementary Figure 5). Cluster comparisons between these HVIs and three other measures of stress ( $T_{\text{leaf}}$  and A) appear in Supplementary Figures 6 and 7.

## Discussion

Our work presented here demonstrates dynamic diurnal changes in HVIs in a commercial vineyard system. Previous studies have used continuous spectral data to evaluate drought stress in sunflowers, olive orchards, and barley at two or three diurnal collection times throughout the day (Gamon et al., 1992; Suárez et al., 2008; Rischbeck et al., 2014). Pinter et al. (1983) evaluated wheat crops at 13 measurement times throughout the day and utilized LANDSAT bands (100 nm spectral resolution) to calculate vegetation indices. The present study collected on-the-ground hyperspectral measurements (2 nm spectral resolution) at up to five diurnal collection times and compared these with conventional measures of stress ( $\Psi_{\text{leaf}}$ ,  $T_{\text{leaf}}$ , A, and  $g_{\text{sw}}$ ) at up to 7 times during several key points in the season. At each of these time points, 12 collection locations were evaluated and compiled across field scale (Figure 1).

Hyperspectral Vegetation Indices (HVIs) are a powerful tool to monitor plant status, and leaf-level measurements can help to inform similar approaches with remote sensing. In this

study, we evaluated leaf-level hyperspectral leaf reflectance data using 88 HVIs and found that 12 demonstrated sensitivity between well-watered and stressed conditions earlier (at 930 or 1130) in the day, while 29 were sensitive later (at 1600) in the afternoon (see Supplementary Figure 1). Interestingly, most indices exhibited a diurnal pattern of detection and only 3 HVIs detected significant differences at all collection times (see Crt2, Crt5, and RBI). This is striking because satellite overpasses that measure spectral signatures usually collect data around solar noon (e.g., HypSIRI passes at  $1030 \pm 30$  min) to minimize shadowing effects, which may miss the time of day when plants are most responsive to water stress. As hyperspectral satellite imaging becomes more readily available, including the use of hyperspectral cameras mounted on unmanned aerial vehicles (UAVs), flight time and HVI selection may influence quality of information about plant status.

HVIs related to chlorophyll and pigmentation (e.g., NPCI from Peñuelas et al., 1993; SRPI from Peñuelas et al., 1995) detected the largest differences between stressed and well-watered plants earlier in the day, while HVIs primarily related to water stress (e.g., NDII1 from Hardinsky and Klemas, 1983; NDWI1 from Gao, 1996; and WI1 from Malthus et al., 1993) had larger differences later in the day (Tables 1 and 2). A handful of HVIs not related to water stress (e.g., mCARI2 from Daughtry et al., 2000; PRI1 from Gamon et al., 1997; and RGRI from Gamon and Surfus, 1999) and with wavelengths in the VIS spectrum (420-700 nm) also found significant differences between stressed and well-watered plants later in the day (Table 2). These HVIs may prove useful for widespread use in viticultural irrigation management to achieve targeted vine stress thresholds using deficit irrigation.

HVIs that were sensitive to differences between block treatments earlier in the day were, in general, designed to detect changes in chlorophyll content (Table 1). Crt2, Crt5, and RBI

detected differences between stressed versus well-watered blocks at all diurnal collection times, and these HVIs utilized bands that were sensitive to chlorophyll a and carotenoid absorbance at 420-445 and 695-700 nm (Carter, 1994; Rodríguez-Pérez et al., 2007). The red absorbance band of chlorophyll around 680 nm is near the red-edge region of the leaf spectrum, which is the transition between low reflectance of visible light and high reflectance of infrared light. Several indices with wavelengths near this region (680-700 nm) detected significant differences between well-watered and stressed blocks (e.g., RGRI, PSRI, SIPI1), while others with wavelengths inside or slightly outside this range (e.g., CARI at 670 and 700 nm) did not detect the same trends (Supplementary Table 2). The success of Crt2, Crt5, and RBI may owe to the inclusion of wavebands in the 420-445 nm region, which spans absorbance maxima of several photosynthetic pigments (Table 1). Alternatively, a reduction in nitrogen content of stressed plants may consequently reduce pigment content that is observed by these HVIs. Utilizing wavebands in this region alone led to detection of significant differences earlier in the day (e.g., 430 nm in NPCI; 435 nm in NPQI), however, inclusion of wavelengths in both pigment absorbance regions (420-445 and 695-700 nm) allowed detection of stressed plants at all diurnal collection times. One complication in these wavebands is the absorbance of several pigments in this region, including the xanthophyll cycle, which is associated with dissipation of excess energy in Photosystem II (Demmig-Adams et al., 1995).

Changes in the xanthophyll cycle may be detected through PRI (Gamon et al., 1992; Wong et al., 2022). Previous studies have observed decreases in  $g_{sw}$  as PRI increases (Suárez et al., 2008), which was observed in this study with some waveband shifts of PRI (see PRI4 in Supplementary Figure 1). Interestingly, these authors observed the strongest correlations

between these parameters at 930 and weaker correlations at 1230. This supports our findings that  $g_{sw}$  is more sensitive to differences between water stress conditions earlier in the day (Figure 3).

In this experiment, irrigation inputs based in part on  $ET_a/ET_{ref}$  values generally created two water stress conditions: well-watered (WW and M) and stressed (S1 and S2), which appear in Figure 2.  $ET_a/ET_{ref}$  is a good proxy for soil moisture, especially in vines strongly dependent on irrigation such as in the Central Valley during summer (Wilson et al., 2020). Conventional measurements collected before stress was imposed were similar across all blocks, which matches observations of  $ET_a/ET_{ref}$  values which were similar at this collection time (Figure 3). During the water stress period, these conventional measures were again collected during an IOP on July 13<sup>th</sup>, approximately three weeks after irrigation treatments were implemented. All conventional measures observed a gradient that corresponded to  $ET_a/ET_{ref}$  (e.g.,  $g_{sw}$ : S2 < S1 < M < WW at nearly all times of day during stress). While S1 and S2 soil moisture content was similar for most of the drying period, there was a slight peak in S1 during this IOP. We attribute this short-term increase in soil moisture to lower stress responses in this block when compared to S2. All plots were irrigated in order to initiate a “recovery” phase. This brought soil moisture levels closer to one another at the end of July. In fact,  $ET_a/ET_{ref}$  converged for all plots on July 30<sup>th</sup>. However, during the final IOP on August 6<sup>th</sup>, there was a dramatic decline in  $ET_a/ET_{ref}$  for stressed blocks, which was not expected for this data collection period. Performing the IOP on July 30<sup>th</sup> or later in the season when  $ET_a/ET_{ref}$  values were closer may have better informed a “recovery” response in these plants. Alternatively, the water stress conditions imposed in June and July may have inflicted permanent damage to the plants (e.g., down-regulation of Photosystem II) that prevented a true “recovery” of stressed plants (Osmond and Grace, 1995). Flexas et al. (1998) concluded that permanent photoinhibition is not extensive in grapevines, even under severe

water stress conditions that greatly reduce photosynthesis, which occurred in this experiment. Thus, we expect that differences during the “after recovery” IOP are due to the separation of soil moisture during data collection.

The stress response occurred as expected based on conventional parameters (Figure 3). During the water stress event measured on July 13<sup>th</sup>, plants from stressed blocks were under “severe” water stress (i.e.,  $g_{sw} < 0.50 \text{ mmol m}^{-2} \text{ s}^{-1}$ ), while well-watered blocks experienced controlled conditions that became more stressed (i.e.,  $g_{sw} < 1.50 \text{ mmol m}^{-2} \text{ s}^{-1}$ ) throughout the day (Flexas and Medrano, 2002). Both  $g_{sw}$  and  $A$  were significantly lower in stressed plants during nearly all data collection points when compared to well-watered plants (Figure 3). We expected that  $T_{leaf}$  would become higher in stressed plants with decreased  $A$  and stomatal closure since excess energy cannot be effectively shuttled through photosynthetic pathways and dissipated via latent heat exchange (Gates, 1964). This physiological cascade has informed remote thermal-based technologies to successfully model grapevine water status (Nieto et al., 2022). However, in the present study, differences in  $T_{leaf}$  between stressed and well-watered plants were less dramatic than  $A$  and  $g_{sw}$  during the water stress event and were somewhat more apparent near solar noon (Figure 3). Still, land surface temperatures (e.g., measured from LANDSAT satellites) for modeling crop water use and stress from space have demonstrated promising results for representing grapevine water status (Kustas et al., 2019; 2022).

As the day progressed,  $\Psi_{leaf}$  dropped steadily (see Figure 3), driven by decreases in relative humidity and increased temperature which increase the vapor pressure deficit and rate of water lost through stomata (Williams and Baeza, 2007). Around 1600, the well-watered plants began to increase water potential, while stress plants continued to respond with lower  $\Psi_{leaf}$  values. At this time, the majority of HVIs that detected significant differences between treatment

conditions were designed as proxies for water content (Table 2). Water absorbs strongly throughout several wavelength regions of the leaf spectrum, including the NIR (819-1450 nm) and MIR (1599-1680) regions. MSI, NDII, and SRWI all utilize wavelengths within these regions to detect water content (Figure 6). Most HVIs with waveband shifts performed similarly to one another (e.g., NDWI1-6 in Supplementary Figure 2). These trends suggest that well-watered plants had greater leaf water content and stronger water absorbance around the NIR and MIR regions (Hunt and Rock, 1989; Alsina et al., 2013). Selection of two bands within the NIR region that were associated with water absorbance also yielded significant sensitivity to water stress, seen in WBI. HVIs that were sensitive to water stress conditions were not exclusive to water content proxy indices (e.g., CUR, mCARI2, RGRI in Table 2). This may be attributed to higher ambient temperature, which was reflected in changes in  $\Psi_{\text{leaf}}$  and  $T_{\text{leaf}}$ . Optimum temperature for photosynthesis in grapevines is 25 to 35C (Zhang et al., 2018). Above this point, Photosystem II is significantly inhibited. In this study, A was reduced around 1600, which may reflect this photodamage (Figure 3).

This study evaluated dozens of HVIs using high spectral resolution leaf-level data that required resources that are not practical for vineyard management operations. Grape growers often intervene with irrigation when plants surpass thresholds of stress that are detected using simple, inexpensive technologies. Ideally, these tools give a representation of field heterogeneity, so that growers can target yield and quality goals while optimizing water usage. Remote sensing tools demonstrate a promising option for tracking crop water use (Kustas et al., 2019; 2022) and stress. One strategy may include a combination of conventional measures of stress ( $\Psi_{\text{leaf}}$ ,  $T_{\text{leaf}}$ , A, and  $g_{\text{sw}}$ ) and HVIs collected during a key time of day when stressed plants are most easily detected. A cluster analysis of conventional parameters and selected HVIs demonstrate the

importance of data collection when these differences are largest (Figures 5 and 7). When considering  $g_{sw}$  and HVIs related to pigment content (e.g., CAI1), differences between well-watered and stressed plants were largest earlier in the day (especially at 930) and these differences gradually decreased as the day progressed (Supplementary Table 3). This was quantified using FMI score, which rates higher scores when clusters are more distinct from one another. In a practical sense, this could be used to determine stress thresholds for growers to use in deciding whether to irrigate. Later in the day (at 1600), indices sensitive to water content and  $\Psi_{leaf}$  demonstrated more distinct clusters of well-watered and stressed plants (e.g. WI2 exhibited perfect separation of treatments in Supplementary Table 4). A grower may decide to measure WI2 and  $\Psi_{leaf}$  at 1600 in order to make an informed decision on vineyard management. We hope that this research adds to the growing understanding of spectral wavebands with specific applications in viticulture (i.e., leaf pigments, stress responses, structure) and to inform both remote sensing and on-the-ground tools (e.g., PRI ground-based sensor; Wong et al., 2022). While some HVIs were highlighted in this discussion, many others appear in Supplementary Tables and Figures that appear at the end.

## References

- Afifi, M., Obenland, D., El-kereamy, A., 2021. The Complexity of Modulating Anthocyanin Biosynthesis Pathway by Deficit Irrigation in Table Grapes. *Frontiers in Plant Science* 12.
- Al-Wassai, F.A., Kalyankar, N.V., 2013. Major Limitations of Satellite images. Bondada, B.R., Matthews, M.A., Shackel, K.A., 2005. Functional xylem in the post-veraison grape berry. *J Exp Bot* 56, 2949–2957. <https://doi.org/10.1093/jxb/eri291>
- Alsina, M.M., Cheng, Riaño, T., D., Whiting, M., Ustin, S. and Smart D.R. (2013). Water status detection in California table grapes: from leaf to airborne. *Precision Agriculture*. J. V. Stafford. Wageningen, The Netherlands, Wageningen Academic Publishers: 824.
- Aoki, M., Yabuki, K., Totsuka, T., 1981. An evaluation of chlorophyll content of leaves based on the spectral reflectivity in several plants. *Research Report of the National Institute of Environmental Studies of Japan* 125–130.
- Aoki, M., Yabuki, K., Totsuka, T., 1981. An evaluation of chlorophyll content of leaves based on the spectral reflectivity in several plants. *Research Report of the National Institute of Environmental Studies of Japan* 125–130.
- Barnes, J.D., Balaguer, L., Manrique, E., Elvira, S., Davison, A.W., 1992. A reappraisal of the use of DMSO for the extraction and determination of chlorophylls a and b in lichens and higher plants. *Environmental and Experimental Botany* 32, 85–100. [https://doi.org/10.1016/0098-8472\(92\)90034-Y](https://doi.org/10.1016/0098-8472(92)90034-Y)
- Blackburn, G.A., 1998. Spectral indices for estimating photosynthetic pigment concentrations: A test using senescent tree leaves. *International Journal of Remote Sensing* 19, 657–675. <https://doi.org/10.1080/014311698215919>
- Birth, G.S., McVey, G.R., 1968. Measuring the Color of Growing Turf with a Reflectance Spectrophotometer. *Agronomy Journal* 60, 640–643. <https://doi.org/10.2134/agronj1968.00021962006000060016x>
- Bravado, B., Hepner, Y., Loinger, C., Cohen, S., Tabacman, H. Effect of crop level and crop load on growth, yield, must and wine composition, and quality of Cabernet Sauvignon. *Am J Enol Vitic* 36(2), 125–131.
- Carter, G.A., 1993. Responses of Leaf Spectral Reflectance to Plant Stress. *American Journal of Botany* 80, 239–243. <https://doi.org/10.1002/j.1537-2197.1993.tb13796.x>
- Carter, G.A., 1994. Ratios of leaf reflectances in narrow wavebands as indicators of plant stress. *International Journal of Remote Sensing* 15, 697–703. <https://doi.org/10.1080/01431169408954109>
- Chappelle, E.W., Kim, M.S., McMurtrey, J.E., 1992. Ratio analysis of reflectance spectra (RARS): An algorithm for the remote estimation of the concentrations of chlorophyll A, chlorophyll B, and carotenoids in soybean leaves. *Remote Sensing of Environment* 39, 239–247. [https://doi.org/10.1016/0034-4257\(92\)90089-3](https://doi.org/10.1016/0034-4257(92)90089-3)
- Coombe, B.G., 1992. Research on Development and Ripening of the Grape Berry. *Am J Enol Vitic*. 43, 101–110. <https://doi.org/10.5344/ajev.1992.43.1.101>
- Datt, B., 1998. Remote Sensing of Chlorophyll a, Chlorophyll b, Chlorophyll a+b, and Total Carotenoid Content in Eucalyptus Leaves. *Remote Sensing of Environment* 66, 111–121. [https://doi.org/10.1016/S0034-4257\(98\)00046-7](https://doi.org/10.1016/S0034-4257(98)00046-7)



- Daughtry, C.S.T., McMurtrey, J.E., Chappelle, E.W., Hunter, W.J., Steiner, J.L., 1996. Measuring crop residue cover using remote sensing techniques. *Theor Appl Climatol* 54, 17–26. <https://doi.org/10.1007/BF00863555>
- Daughtry, C.S.T., Walthall, C.L., Kim, M.S., de Colstoun, E.B., McMurtrey, J.E., 2000. Estimating Corn Leaf Chlorophyll Concentration from Leaf and Canopy Reflectance. *Remote Sensing of Environment* 74, 229–239. [https://doi.org/10.1016/S0034-4257\(00\)00113-9](https://doi.org/10.1016/S0034-4257(00)00113-9)
- Daughtry, C.S.T., 2001. Discriminating Crop Residues from Soil by Shortwave Infrared Reflectance. *Agronomy Journal* 93, 125–131. <https://doi.org/10.2134/agronj2001.931125x>
- Dash, J., Curran, P.J., 2004. The MERIS terrestrial chlorophyll index. *International Journal of Remote Sensing* 25, 5403–5413. <https://doi.org/10.1080/0143116042000274015>
- Demmig-Adams, B., Adams, W.I., Logan, B.A., Verhoeven, A.S., 1995. Xanthophyll Cycle-Dependent Energy Dissipation and Flexible Photosystem II Efficiency in Plants Acclimated to Light Stress. *Functional Plant Biol.* 22, 249–260. <https://doi.org/10.1071/pp9950249>
- Flexas, J., Escalona, J.M., Medrano, H., 1998. Down-regulation of photosynthesis by drought under field conditions in grapevine leaves. *Functional Plant Biol.* 25, 893. <https://doi.org/10.1071/PP98054>
- Flexas, J., Medrano, H., 2002. Drought-inhibition of photosynthesis in C3 plants: stomatal and non-stomatal limitations revisited. *Ann Bot* 89, 183–189. <https://doi.org/10.1093/aob/mcf027>
- Gamon, J.A., Peñuelas, J., Field, C.B., 1992. A narrow-waveband spectral index that tracks diurnal changes in photosynthetic efficiency. *Remote Sensing of Environment* 41, 35–44. [https://doi.org/10.1016/0034-4257\(92\)90059-S](https://doi.org/10.1016/0034-4257(92)90059-S)
- Gamon, J.A., Serrano, L., Surfus, J.S., 1997. The photochemical reflectance index: an optical indicator of photosynthetic radiation use efficiency across species, functional types, and nutrient levels. *Oecologia* 112, 492–501. <https://doi.org/10.1007/s004420050337>
- Gamon, J.A., Surfus, J.S., 1999. Assessing leaf pigment content and activity with a reflectometer. *New Phytologist* 143, 105–117. <https://doi.org/10.1046/j.1469-8137.1999.00424.x>
- Gao, B., 1996. NDWI—A normalized difference water index for remote sensing of vegetation liquid water from space. *Remote Sensing of Environment* 58, 257–266. [https://doi.org/10.1016/S0034-4257\(96\)00067-3](https://doi.org/10.1016/S0034-4257(96)00067-3)
- Gates, D.M., 1964. Leaf Temperature and Transpiration. *Agronomy Journal* 56, 273–277. <https://doi.org/10.2134/agronj1964.00021962005600030007x>
- Gates, D.M., Keegan, H.J., Schleter, J.C., Weidner, V.R., 1965. Spectral Properties of Plants. *Appl. Opt.*, AO 4, 11–20. <https://doi.org/10.1364/AO.4.000011>
- Gitelson, A., Merzlyak, M.N., 1994. Spectral Reflectance Changes Associated with Autumn Senescence of *Aesculus hippocastanum* L. and *Acer platanoides* L. Leaves. Spectral Features and Relation to Chlorophyll Estimation. *Journal of Plant Physiology* 143, 286–292. [https://doi.org/10.1016/S0176-1617\(11\)81633-0](https://doi.org/10.1016/S0176-1617(11)81633-0)

- Gitelson, A.A., Kaufman, Y.J., Merzlyak, M.N., 1996. Use of a green channel in remote sensing of global vegetation from EOS-MODIS. *Remote Sensing of Environment* 58, 289–298. [https://doi.org/10.1016/S0034-4257\(96\)00072-7](https://doi.org/10.1016/S0034-4257(96)00072-7)
- Gitelson, A. A., Merzlyak, M.N., Chivkunova, O.B., 2001a. Optical properties and nondestructive estimation of anthocyanin content in plant leaves. *Photochem Photobiol* 74, 38–45. [https://doi.org/10.1562/0031-8655\(2001\)074<0038:opaneo>2.0.co;2](https://doi.org/10.1562/0031-8655(2001)074<0038:opaneo>2.0.co;2)
- Gitelson, Anatoly A, Merzlyak, M.N., Zur, Y., Stark, R., Gritz, U., 2001b. Non-destructive and remote sensing techniques for estimation of vegetation status. *Papers in Natural Resources* 273, 7.
- Gitelson, A.A., Gritz, Y., Merzlyak, M.N., 2003. Relationships between leaf chlorophyll content and spectral reflectance and algorithms for non-destructive chlorophyll assessment in higher plant leaves. *Journal of Plant Physiology* 160, 271–282. <https://doi.org/10.1078/0176-1617-00887>
- Gitelson, A.A., Viña, A., Ciganda, V., Rundquist, D.C., Arkebauer, T.J., 2005. Remote estimation of canopy chlorophyll content in crops. *Geophysical Research Letters* 32. <https://doi.org/10.1029/2005GL022688>
- Gitelson, A.A., Keydan, G.P., Merzlyak, M.N., 2006. Three-band model for noninvasive estimation of chlorophyll, carotenoids, and anthocyanin contents in higher plant leaves. *Geophysical Research Letters* 33. <https://doi.org/10.1029/2006GL026457>
- Haboudane, D., Miller, J.R., Tremblay, N., Zarco-Tejada, P.J., Dextraze, L., 2002. Integrated narrow-band vegetation indices for prediction of crop chlorophyll content for application to precision agriculture. *Remote Sensing of Environment* 81, 416–426. [https://doi.org/10.1016/S0034-4257\(02\)00018-4](https://doi.org/10.1016/S0034-4257(02)00018-4)
- Haboudane, D., Miller, J.R., Pattey, E., Zarco-Tejada, P.J., Strachan, I.B., 2004. Hyperspectral vegetation indices and novel algorithms for predicting green LAI of crop canopies: Modeling and validation in the context of precision agriculture. *Remote Sensing of Environment* 90, 337–352. <https://doi.org/10.1016/j.rse.2003.12.013>
- Hardinsky, M., Klemas, V., 1983. The influence of soil salinity, growth form, and leaf moisture on the spectral radiance of *Spartina Alterniflora* canopies. *Photogrammetric Engineering and Remote Sensing* 48, 77–84.
- Hunt, R.E., Rock, B.N., Nobel, P.S., 1987. Measurement of leaf relative water content by infrared reflectance. *Remote Sensing of Environment* 22, 429–435. [https://doi.org/10.1016/0034-4257\(87\)90094-0](https://doi.org/10.1016/0034-4257(87)90094-0)
- Hunt, E.R., Rock, B.N., 1989. Detection of changes in leaf water content using Near- and Middle-Infrared reflectances. *Remote Sensing of Environment* 30, 43–54. [https://doi.org/10.1016/0034-4257\(89\)90046-1](https://doi.org/10.1016/0034-4257(89)90046-1)
- HyspIRI Mission Concept Team. (2018). (rep.). *HyspIRI Final Report* (pp. 1–91). Pasadena, CA.
- IPCC, 2021: *Climate Change 2021: The Physical Science Basis. Contribution of Working Group*

*I to the Sixth Assessment Report of the Intergovernmental Panel on Climate Change* [Masson-Delmotte, V., P. Zhai, A. Pirani, S.L. Connors, C. Péan, S. Berger, N. Caud, Y. Chen, L. Goldfarb, M.I. Gomis, M. Huang, K. Leitzell, E. Lonnoy, J.B.R. Matthews, T.K. Maycock, T. Waterfield, O. Yelekçi, R. Yu, and B. Zhou (eds.)]. Cambridge University Press, Cambridge, United Kingdom and New York, NY, USA, In press, doi:[10.1017/9781009157896](https://doi.org/10.1017/9781009157896).

- Josep, P., Baret, F., Iolanda, F., 1995. Semi-Empirical Indices to Assess Carotenoids/Chlorophyll-a Ratio from Leaf Spectral Reflectance. *Photosynthetica* 31, 221–230.
- Jurgens, C., 1997. The modified normalized difference vegetation index (mNDVI) a new index to determine frost damages in agriculture based on Landsat TM data. *International Journal of Remote Sensing* 18, 3583–3594. <https://doi.org/10.1080/014311697216810>
- Johnson, R., Cody, B.A., 2015. California Agricultural Production and Irrigated Water Use. Miras-Avalos, J., Araujo, E., 2021. Optimization of Vineyard Water Management: Challenges, Strategies, and Perspectives. *Water* 13, 746. <https://doi.org/10.3390/w13060746>
- Kim, M.S., 1994. The use of narrow spectral bands for improving remote sensing estimations of fractional absorbed photosynthetically active radiation (fapar).
- Knipper, K.R., Kustas, W.P., Anderson, M.C., Alsina, M.M., Hain, C.R., Alfieri, J.G., Prueger, J.H., Gao, F., McKee, L.G., Sanchez, L.A., 2019. Using High-Spatiotemporal Thermal Satellite ET Retrievals for Operational Water Use and Stress Monitoring in a California Vineyard. *Remote Sensing* 11, 2124. <https://doi.org/10.3390/rs11182124>
- Knipper, K.R., Kustas, W.P., Anderson, M.C., Nieto, H., Alfieri, J.G., Prueger, J.H., Hain, C.R., Gao, F., McKee, L.G., Alsina, M.M., Sanchez, L., 2020. Using high-spatiotemporal thermal satellite ET retrievals to monitor water use over California vineyards of different climate, vine variety and trellis design. *Agricultural Water Management* 241, 106361. <https://doi.org/10.1016/j.agwat.2020.106361>
- Kustas, W.P., Anderson, M.C., Alfieri, J.G., Knipper, K., Torres-Rua, A., Parry, C.K., Nieto, H., Agam, N., White, W.A., Gao, F., McKee, L., Prueger, J.H., Hipps, L.E., Los, S., Alsina, M.M., Sanchez, L., Sams, B., Dokoozlian, N., McKee, M., Jones, S., Yang, Y., Wilson, T.G., Lei, F., McElrone, A., Heitman, J.L., Howard, A.M., Post, K., Melton, F., Hain, C., 2018. The Grape Remote Sensing Atmospheric Profile and Evapotranspiration Experiment. *Bulletin of the American Meteorological Society* 99, 1791–1812. <https://doi.org/10.1175/BAMS-D-16-0244.1>
- Kustas, W.P., Agam, N., Ortega-Farias, S., 2019. Forward to the GRAPEX special issue. *Irrig Sci* 37, 221–226. <https://doi.org/10.1007/s00271-019-00633-7>
- Kustas, W.P., McElrone, A.J., Agam, N., Knipper, K., 2022. From vine to vineyard: the GRAPEX multi-scale remote sensing experiment for improving vineyard irrigation management. *Irrig Sci* 40, 435–444. <https://doi.org/10.1007/s00271-022-00816-9>
- Malthus, T.J., Andrieu, B., Danson, F.M., Jaggard, K.W., Steven, M.D., 1993. Candidate high spectral resolution infrared indices for crop cover. *Remote Sensing of Environment* 46, 204–212. [https://doi.org/10.1016/0034-4257\(93\)90095-F](https://doi.org/10.1016/0034-4257(93)90095-F)
- Merzlyak, M.N., Gitelson, A.A., Chivkunova, O.B., Rakitin, V.YU., 1999. Non-destructive

- optical detection of pigment changes during leaf senescence and fruit ripening. *Physiologia Plantarum* 106, 135–141. <https://doi.org/10.1034/j.1399-3054.1999.106119.x>
- Mirás-Avalos, J.M., Silva Araujo, E., 2021. Optimization of Vineyard Water Management: Challenges, Strategies, and Perspectives. <https://doi.org/10.3390/w13060746>
- Mount, J., Hanak, E., Bardeen, S., Escriva-Bou, A., Peterson, C., Ayres, A., Cole, S., Gray, B., Joaquin-Morales, Z., Rosser, A., Sencan, G., n.d. Priorities for California's Water: Thriving with Less.
- Nieto, H., Alsina, M.M., Kustas, W.P., García-Tejera, O., Chen, F., Bambach, N., Gao, F., Alfieri, J.G., Hipps, L.E., Prueger, J.H., McKee, L.G., Zahn, E., Bou-Zeid, E., McElrone, A.J., Castro, S.J., Dokoozlian, N., 2022. Evaluating different metrics from the thermal-based two-source energy balance model for monitoring grapevine water stress. *Irrig Sci* 40, 697–713. <https://doi.org/10.1007/s00271-022-00790-2>
- Ojeda H., 2007. Irrigation qualitative de précision de la vigne. *Le Progrès Agricole et Viticole*, 127(7), 133–141.
- Osmond, C.B., Grace, S.C., 1995. Perspectives on photoinhibition and photorespiration in the field: quintessential inefficiencies of the light and dark reactions of photosynthesis? *Journal of Experimental Botany* 46, 1351-1362.
- Pádua, L., Adão, T., Sousa, A., Peres, E., Sousa, J. 2020. Individual Grapevine Analysis in a Multi-Temporal Context Using UAV-Based Multi-Sensor Imagery. *Remote Sens* 12 139.
- Peñuelas, J., Gamon, J.A., Griffin, K.L., Field, C.B., 1993a. Assessing community type, plant biomass, pigment composition, and photosynthetic efficiency of aquatic vegetation from spectral reflectance. *Remote Sensing of Environment* 46, 110–118. [https://doi.org/10.1016/0034-4257\(93\)90088-F](https://doi.org/10.1016/0034-4257(93)90088-F)
- Peñuelas, J., Filella, I., Biel, C., Serrano, L., Savé, R., 1993b. The reflectance at the 950–970 nm region as an indicator of plant water status. *International Journal of Remote Sensing* 14, 1887–1905. <https://doi.org/10.1080/01431169308954010>
- Peñuelas, J., Frederic, B., Filella, I., 1995. Semi-Empirical Indices to Assess Carotenoids/Chlorophyll-a Ratio from Leaf Spectral Reflectance. *Photosynthetica* 31, 221–230.
- Peñuelas, J., Pinol, J., Ogaya, R., Filella, I., 1997. Estimation of plant water concentration by the reflectance Water Index WI (R900/R970). *International Journal of Remote Sensing* 18, 2869–2875. <https://doi.org/10.1080/014311697217396>
- Pinter, P.J., Jackson, R.D., Idso, S.B., Reginato, R.J., 1983. Diurnal Patterns of Wheat Spectral Reflectances. *IEEE Transactions on Geoscience and Remote Sensing* GE-21, 156–163. <https://doi.org/10.1109/TGRS.1983.350484>
- Poblete, T., Ortega-Farías, S., Moreno, M.A., Bardeen, M., 2017. Artificial Neural Network to Predict Vine Water Status Spatial Variability Using Multispectral Information Obtained from an Unmanned Aerial Vehicle (UAV). *Sensors* 17, 2488. <https://doi.org/10.3390/s17112488>
- Rischbeck, P., Baresel, P., Elsayed, S., Mistele, B., Schmidhalter, U., Rischbeck, P., Baresel, P., Elsayed, S., Mistele, B., Schmidhalter, U., 2014. Development of a diurnal dehydration index for spring barley phenotyping. *Functional Plant Biol.* 41, 1249–1260. <https://doi.org/10.1071/FP14069>

- Rock, B.N., Williams, D.L., Vogelmann, J.E., 1985. Field and airborne spectral characterization of suspected acid deposition damage in red spruce (*Picea rubens*). *Proc. Symp. on Machine Processing of Remotely Sensed Data*. 71–81.
- Rodríguez-Pérez, J.R., Riaño, D., Carlisle, E., Ustin, S., Smart, D.R., 2007. Evaluation of Hyperspectral Reflectance Indexes to Detect Grapevine Water Status in Vineyards 16.
- Rouse, W., Haas, R.H., n.d. Monitoring vegetation systems in the great plains with ERTS.
- Uto, K., Kosugi, Y., 2012. Hyperspectral Manipulation for the Water Stress Evaluation of Plants. *Contemporary Materials* 1, 18–25. <https://doi.org/10.7251/COM1201018U>
- Roujean, J.-L., Breon, F.-M., 1995. Estimating PAR absorbed by vegetation from bidirectional reflectance measurements. *Remote Sensing of Environment* 51, 375–384. [https://doi.org/10.1016/0034-4257\(94\)00114-3](https://doi.org/10.1016/0034-4257(94)00114-3)
- Serrano, L., Peñuelas, J., Ustin, S.L., 2002. Remote sensing of nitrogen and lignin in Mediterranean vegetation from AVIRIS data: Decomposing biochemical from structural signals. *Remote Sensing of Environment* 81, 355–364. [https://doi.org/10.1016/S0034-4257\(02\)00011-1](https://doi.org/10.1016/S0034-4257(02)00011-1)
- Sims, D.A., Gamon, J.A., 2002. Relationships between leaf pigment content and spectral reflectance across a wide range of species, leaf structures and developmental stages. *Remote Sensing of Environment* 81, 337–354. [https://doi.org/10.1016/S0034-4257\(02\)00010-X](https://doi.org/10.1016/S0034-4257(02)00010-X)
- Sivanpillai, R., Jacobs, K.M., Mattilio, C.M., Piskorski, E.V., 2021. Rapid flood inundation mapping by differencing water indices from pre- and post-flood Landsat images. *Front. Earth Sci.* 15, 1–11. <https://doi.org/10.1007/s11707-020-0818-0>
- Suárez, L., Zarco-Tejada, P.J., Sepulcre-Cantó, G., Pérez-Priego, O., Miller, J.R., Jiménez-Muñoz, J.C., Sobrino, J., 2008. Assessing canopy PRI for water stress detection with diurnal airborne imagery. *Remote Sensing of Environment, Soil Moisture Experiments 2004 (SMEX04) Special Issue* 112, 560–575. <https://doi.org/10.1016/j.rse.2007.05.009>
- Tang, Z., Jin, Y., Alsina, M.M., McElrone, A.J., Bambach, N., Kustas, W.P., 2022. Vine water status mapping with multispectral UAV imagery and machine learning. *Irrig Sci* 40, 715–730. <https://doi.org/10.1007/s00271-022-00788-w>
- Tucker, C.J., 1979. Red and photographic infrared linear combinations for monitoring vegetation. *Remote Sensing of Environment* 8, 127–150. [https://doi.org/10.1016/0034-4257\(79\)90013-0](https://doi.org/10.1016/0034-4257(79)90013-0)
- U.S. Department of Agriculture (USDA), Economic Research Service (ERS), Food Dollar Series, November 2022.
- Vogelmann, J.E., Rock, B.N., Moss, D.M., 1993. Red edge spectral measurements from sugar maple leaves. *International Journal of Remote Sensing* 14, 1563–1575. <https://doi.org/10.1080/01431169308953986>
- Vogelmann, J.E., Rock, B.N., Moss, D.M., 1993. Red edge spectral measurements from sugar maple leaves. *International Journal of Remote Sensing* 14, 1563–1575. <https://doi.org/10.1080/01431169308953986>
- Williams, L.E., Baeza, P., 2007. Relationships among Ambient Temperature and Vapor Pressure

- Deficit and Leaf and Stem Water Potentials of Fully Irrigated, Field-Grown Grapevines. *Am J Enol Vitic.* 58, 173–181. <https://doi.org/10.5344/ajev.2007.58.2.173>
- Williams, L.E., Baeza, P., Vaughn, P., 2012. Midday measurements of leaf water potential and stomatal conductance are highly correlated with daily water use of Thompson Seedless grapevines. *Irrig Sci* 30, 201–212. <https://doi.org/10.1007/s00271-011-0276-2>
- Williams, L.E., 2017. Physiological tools to assess vine water status for use in vineyard irrigation management: review and update. *Acta Hort.* 151–166. <https://doi.org/10.17660/ActaHortic.2017.1157.24>
- Williams, L.E., Heymann, H., 2017. Effects of applied water amounts and trellis/training system on grapevine water relations, berry characteristics, productivity and wine composition of ‘Cabernet Sauvignon.’ *Acta Hort.* 413–426. <https://doi.org/10.17660/ActaHortic.2017.1150.58>
- Wilson, T.G., Kustas, W.P., Alfieri, J.G., Anderson, M.C., Gao, F., Prueger, J.H., McKee, L.G., Alsina, M.M., Sanchez, L.A., Alstad, K.P., 2020. Relationships between soil water content, evapotranspiration, and irrigation measurements in a California drip-irrigated Pinot noir vineyard. *Agricultural Water Management* 237, 106186. <https://doi.org/10.1016/j.agwat.2020.106186>
- Wong, C.Y.S., Bambach, N.E., Alsina, M.M., McElrone, A.J., Jones, T., Buckley, T.N., Kustas, W.P., Magney, T.S., 2022. Detecting short-term stress and recovery events in a vineyard using tower-based remote sensing of photochemical reflectance index (PRI). *Irrig Sci* 40, 683–696. <https://doi.org/10.1007/s00271-022-00777-z>
- Wu, C., Niu, Z., Tang, Q., Huang, W., 2008. Estimating chlorophyll content from hyperspectral vegetation indices: Modeling and validation. *Agricultural and Forest Meteorology* 148, 1230–1241. <https://doi.org/10.1016/j.agrformet.2008.03.005>
- Zarco-Tejada, P.J., Miller, J.R., Mohammed, G.H., Noland, T.L., 2000. Chlorophyll Fluorescence Effects on Vegetation Apparent Reflectance: I. Leaf-Level Measurements and Model Simulation. *Remote Sensing of Environment* 74, 582–595. [https://doi.org/10.1016/S0034-4257\(00\)00148-6](https://doi.org/10.1016/S0034-4257(00)00148-6)
- Zarco-Tejada, P.J., Ustin, S.L., 2001. Modeling canopy water content for carbon estimates from MODIS data at land EOS validation sites, in: *IGARSS 2001. Scanning the Present and Resolving the Future. Proceedings. IEEE 2001 International Geoscience and Remote Sensing Symposium (Cat. No.01CH37217)*. Presented at the IGARSS 2001. Scanning the Present and Resolving the Future. Proceedings. IEEE 2001 International Geoscience and Remote Sensing Symposium (Cat. No.01CH37217), pp. 342–344 vol.1. <https://doi.org/10.1109/IGARSS.2001.976152>
- Zhang, K., Chen, B., Hao, Y., Yang, R., Wang, Y., 2018. Effects of short-term heat stress on PSII and subsequent recovery for senescent leaves of *Vitis vinifera* L. cv. Red Globe. *Journal of Integrative Agriculture* 17, 2683–2693. [https://doi.org/10.1016/S2095-3119\(18\)62143-4](https://doi.org/10.1016/S2095-3119(18)62143-4)
- Zhou, J.-J., Zhang, Y.-H., Han, Z.-M., Liu, X.-Y., Jian, Y.-F., Hu, C.-G., Dian, Y.-Y., 2021. Evaluating the Performance of Hyperspectral Leaf Reflectance to Detect Water Stress and Estimation of Photosynthetic Capacities. *Remote Sensing* 13, 2160. <https://doi.org/10.3390/rs13112160>
- Zur, Y., Gitelson, A.A., Chivkunova, O.B., Merzlyak, M.N., 2000. The spectral contribution of carotenoids to light absorption and reflectance in green leaves 2, 8.

## Tables

**Table 1.** Hyperspectral vegetation indices (HVIs) that detected differences between stressed versus well-watered and mildly stressed blocks earlier in the day. HVI values are calculated using reflectance measured at wavelengths which appear along the bottom. Wavelength ranges are grouped based on leaf properties described in source material for HVI determination.

Leaf property	Chlr a, Chlr b, Car, Xan	Chlr a only	NIR	Source
Index	Crt2	Crt2		Carter 1994
	Crt5	Crt5		
	mSR1		mSR1	Sims and Gamon 2002
	NPCI	NPCI		Peñuelas et al. 1993a
	NPQI			Barnes et al. 1992, Josep et al. 1995
	PSRI	PSRI	PSRI	Merzlyak et al. 1999
	RBI	RBI		Rodríguez-Perez et al. 2007
	SIPI1	SIPI1	SIPI1	
	SIPI2		SIPI2	Peñuelas et al. 1995
	SRPI	SRPI		
Wavelength (nm)	415–500	680–700	750–800	

\*Chlr = chlorophyll, Car = carotenoids, NIR = near infrared, Xan = xanthophylls

**Table 2.** Hyperspectral vegetation indices (HVIs) that detected differences between stressed versus well-watered and mildly stressed blocks later in the day. HVI values are calculated using reflectance measured at wavelengths which appear along the bottom. Wavelength ranges are grouped based on leaf properties described in source material for HVI determination.

Leaf property	Chlr a, car	Reference, xanthophylls	Chlr a only	NIR	EWT	Avoid cellulose	NIR	MIR	Nitrogen	Lignin	Source	
Index	Crt2		Crt2								Carter 1994	
	Crt5		Crt5								Zarco-Tejada et al. 2000	
			CUR								Daughtry et al. 2000	
		mCAR12	mCAR12	mCAR12							Hunt and Rock 1989	
					MSI1						Rock et al. 1985	
					MSI2						Hardinsky and Klemas 1983	
					NDIII1						NDLI	Serrano et al. 2002
					NDIII2							
					NDIII3							
					NDWI1		NDWI1					
					NDWI2							
					NDWI3		NDWI3					Gao 1996
Wavelength (nm)	420–445	500	680–700	819-970	1070-1100	1241-1340	1450	1599-1680	1510	1754		

\*Chlr a = chlorophyll a, car = carotenoids, NIR = near infrared, EWT = equivalent water thickness, MIR = middle infrared, Xan = xanthophylls



**Table 2 (cont'd).**

Leaf property	Chlr a, car xanthophylls	Reference, Chlr a only	NIR	EWT	Avoid cellulose	NIR	MIR	Nitrogen	Lignin	Source
			NDWI4							
				NDWI5		NDWI5				Gao 1996
					NDWI6	NDWI6				
	PRI1 PRI2									Gamon et al. 1997
	RBI	RBI								Rodriguez-Perez et al. 2007
		RGRI	RGRI							Gamon and Surfus 1999
				SR4	SR4					
				SRWI1	SRWI1					Zarco-
				SRWI2	SRWI2					Tejada and Ustin 2001
				SRWI3	SRWI3					
			WBI							Peñuelas et al. 1993b, Peñuelas et al. 1997
					WI1					
			WI2		WI2					Malthus et al. 1993
	WI3	WI3								
Wavelength (nm)	420-445	500	680-700	819-970	1070-1100	1241-1340	1450	1599-1680	1510	1754

**Supplementary Table 1.** Hyperspectral vegetations indices (HVIs) evaluated for this study. HVIs are assigned a type, subtype, and level based on initial formulation of the index in the source material. HVIs are calculated based on hyperspectral reflectance data collected at the Ripperdan 720 vineyard in Madera, CA, from June to August, 2018. Key time of day is based on significant differences between stressed versus well-watered and moderately stressed blocks during water stress which was imposed on July 13<sup>th</sup>. Early HVIs are sensitive to these block differences at 930 and/or 1130. Late HVIs are sensitive to these block differences at 1600.

Type	Subtype	Level	Key time		Index name	Formula	Source
			of day	Shorthand			
Pigment	Anthocyanins	Leaf		Anthocyanin	ACI	$\frac{R_{550}}{R_{800}}$	Aoki et al. 1981
				Anthocyanin	ARI1	$\frac{1}{\frac{1}{R_{800}} - \frac{1}{R_{700}}}$	Gielson et al.
				Reflectance Index	ARI2	$R_{800} * \left( \frac{1}{R_{550}} - \frac{1}{R_{700}} \right)$	2001a, 2001b
Structure	Cellulose, Lignin	Early		Cellulose	CAI1	$100 * (0.5 * (R_{2031} + R_{2211}) - R_{2101})$	Daughtry 2001,
				Absorption Index	CAI2	$0.5 * (R_{2000} + R_{2200}) - R_{2100}$	Daughtry et al. 1996
Pigment	Chlorophyll	Canopy		Chlorophyll	CARI		
				Absorption Ratio Index		$(R_{700} - R_{670}) - 0.2 * (R_{700} + R_{550})$	Kim 1994

		Chlorophyll Index		$\frac{R_{730}}{R_{530}} - 1$	
Leaf,		- Green	CI green		Gitelson et al. 2005
Canopy		Chlorophyll Index - Red Edge	CI red edge	$\frac{R_{850}}{R_{730}} - 1$	
Carotenoids		Carotenoid	CRI1	$\frac{1}{R_{510}} - \frac{1}{R_{550}}$	Gitelson et al.
		Reflectance Index	CRI2	$\frac{1}{R_{510}} - \frac{1}{R_{700}}$	
			Crt1	$\frac{R_{605}}{R_{760}}$	
		Leaf		Crt2	$\frac{R_{695}}{R_{420}}$
	Leaf		Crt3	$\frac{R_{695}}{R_{676}}$	Carter 1994
		Carter Index	Crt4	$\frac{R_{695}}{R_{760}}$	
Pigment, Stress	Chlorophyll		Crt5	$\frac{R_{700}}{R_{420}}$	

				Crt6	$\frac{R_{710}}{R_{760}}$	
	Chlorophyll a	Late	Curvature Index	CUR	$\frac{R_{675}}{R_{690}} * R_{683}^2$	Zarco-Tejada et al. 2000
Pigment	Chlorophyll		Datt Chlorophyll Index	DattSCI	$\frac{R_{850} - R_{710}}{R_{850} - R_{680}}$	Datt 1998
Color	Plant (turf)		Difference Vegetative Index	DVI	$R_{880} - R_{673}$	Birth and McVey 1968
Pigment, Biomass	Chlorophyll		Enhanced Vegetation Index	EVI	$2.5 * \frac{R_{858} - R_{645}}{R_{858} + 6 * R_{645} - 7.5 * R_{469}}$	Huete et al. 1999
	Chlorophyll a	Canopy	Gielson Merzlyak Index	GMI1	$\frac{R_{750}}{R_{550}}$	Gitelson et al. 1996
Pigment			Modified Anthocyanin Reflectance Index	GMI2	$\frac{R_{750}}{R_{700}}$	
	Anthocyanin	Leaf		mARI	$\frac{1}{R_{500}} - \frac{1}{R_{700}} * R_{800}$	Gitelson et al. 2006

Pigment, Biomass	Chlorophyll,	Leaf,	Modified Chlorophyll	mCARI1	$(R_{700} - R_{670}) - 0.2 * (R_{700} + R_{550})$	Daughtry et al.
	LAI	Canopy	Absorption in Reflectance Index	mCARI2	$1.2 * (2.5 * (R_{800} - R_{670}) - 1.3 * (R_{800} + R_{550}))$	2000
Pigment, Stress	Chlorophyll	Leaf	Moisture Stress	MSI1	$\frac{R_{1599}}{R_{819}}$	Hunt and Rock 1989
Canopy	Canopy	Late	Index	MSI2	$\frac{R_{1650}}{R_{835}}$	Rock et al. 1985
Pigment	Chlorophyll	Leaf,	Ratio Index	mSR2	$\frac{\frac{R_{845}}{R_{665}} - 1}{\sqrt{\frac{R_{845}}{R_{665}} + 1}}}$	Wu et al. 2008

	Canopy	MERIS Terrestrial Chlorophyll Index	MTCI	$\frac{R_{754} - R_{709}}{R_{709} - R_{681}}$	Dash and Curran 2004		
Biomass	LAI	Canopy	Modified Triangular	$1.2 * (1.2 * (R_{880} - R_{554}) - 2.5 * (R_{758} - R_{554}))$	Haboudane et al.		
			Vegetation Index	$1.5 * (2.5 * (R_{800} - R_{550}) - 2.5 * (R_{670} - R_{550}))$	2004		
			mTVI2				
	Leaf, Late	Normalized	NDI11	$\frac{R_{819} - R_{1640}}{R_{819} + R_{1640}}$			
Water	LWC	Plant (marsh)	Late	Difference Infrared Index	NDI12	$\frac{R_{819} - R_{1649}}{R_{819} + R_{1649}}$	Hardisky and Klemas 1983
			Late	Normalized	NDI13	$\frac{R_{835} - R_{1650}}{R_{835} + R_{1650}}$	
Structure	Lignin	Canopy	Normalized				
			Late	Difference Lignin Index	NDLI	$\frac{\log \frac{1}{R_{1754}} - \log \frac{1}{R_{1680}}}{\log \frac{1}{R_{1754}} - \log \frac{1}{R_{1680}}}$	
			Late	Normalized			
	Nitrogen		Late	Difference Nitrogen Index	NDNI	$\frac{\log \frac{1}{R_{1510}} - \log \frac{1}{R_{1680}}}{\log \frac{1}{R_{1510}} - \log \frac{1}{R_{1680}}}$	Serrano et al. 2002

				NDVII	$\frac{R_{800} - R_{673}}{R_{800} + R_{673}}$	
				NDVI2	$\frac{R_{800} - R_{680}}{R_{800} + R_{680}}$	
Pigment, Biomass	Chlorophyll, LAI	Normalized Difference Vegetation Index	NDVI3	NDVI4	$\frac{R_{845} - R_{665}}{R_{845} + R_{665}}$	Tucker et al. 1979
					$\frac{R_{870} - R_{673}}{R_{870} + R_{673}}$	
				NDVI5	$\frac{R_{884} - R_{680}}{R_{884} + R_{680}}$	
				NDVI6	$\frac{R_{895} - R_{675}}{R_{895} + R_{675}}$	
			Late	NDWI1	$\frac{R_{860} - R_{1241}}{R_{860} + R_{1241}}$	
Water	LWT	Normalized Difference Water Index	Late	NDWI2	$\frac{R_{860} - R_{1640}}{R_{860} + R_{1640}}$	Gao 1996
			Late	NDWI3	$\frac{R_{860} - R_{2130}}{R_{860} + R_{2130}}$	
			Late	NDWI4	$\frac{R_{870} - R_{1260}}{R_{870} + R_{1260}}$	

	Late		NDWI5	$\frac{R_{1100} - R_{1450}}{R_{1100} + R_{1450}}$	
	Late		NDWI6	$\frac{R_{1280} - R_{1450}}{R_{1280} + R_{1450}}$	
		Normalized to total			
	Plant	Early	NPPI	$\frac{R_{680} - R_{430}}{R_{680} + R_{430}}$	Peñuelas et al. 1993a
			Chlorophyll Index		
		Normalized			
	Leaf	Early	NPQI	$\frac{R_{415} - R_{435}}{R_{415} + R_{435}}$	Barnes et al. 1992, Josep et al. 1995
			Index		
Pigment		Late	PR1	$\frac{R_{531} - R_{570}}{R_{531} + R_{570}}$	
		Late	PR2	$\frac{R_{528} - R_{567}}{R_{528} + R_{567}}$	
	Xanthophyll	Leaf	PR3	$\frac{R_{538} - R_{567}}{R_{538} + R_{567}}$	Gannon et al. 1997
		Late	PR4	$\frac{R_{570} - R_{539}}{R_{570} + R_{539}}$	



	Pigment Specific		
Chlorophyll a	Normalized Difference Index - Chlorophyll a	PSNDA	$\frac{R_{800} - R_{675}}{R_{800} + R_{675}}$
	Pigment Specific		
Chlorophyll b	Normalized Difference Index - Chlorophyll b	PSNDb	$\frac{R_{800} - R_{650}}{R_{800} + R_{650}}$
	Pigment Specific		
Carotenoids	Normalized Difference Index - Carotenoids	PSNDc	$\frac{R_{800} - R_{500}}{R_{800} + R_{500}}$
Carotenoids, Chlorophyll	Plant Senescence Early Reflectance Index	PSRI	$\frac{R_{680} - R_{500}}{R_{750}}$
	Pigment Specific		
Chlorophyll a	Simple Ratio Index - Chlorophyll a	PSSRa	$\frac{R_{800}}{R_{675}}$

Merzlyak et al.

1999

Blackburn 1998

	Pigment Specific		
Chlorophyll b	Simple Ratio Index - Chlorophyll b	PSSRb	$\frac{R_{800}}{R_{650}}$
	Pigment Specific		
Carotenoids	Simple Ratio Index - Carotenoids	PSSRc	$\frac{R_{800}}{R_{470}}$
	Ratio Analysis of		
Chlorophyll a	Reflectance Spectra Index - Chlorophyll a	RARSa	$\frac{R_{675}}{R_{700}}$
	Ratio Analysis of		
Chlorophyll b	Reflectance Spectra Index - Chlorophyll b	RARSb	$\frac{R_{675}}{R_{650} * R_{700}}$
	Ratio Analysis of		
Carotenoids	Reflectance Spectra Index - Carotenoids	RARSc	$\frac{R_{760}}{R_{500}}$

Chappelle et al.  
1992

Chlorophyll	Leaf, Canopy	Early, Late	Red/Blue Pigment Index	RBI	$\frac{R_{695}}{R_{445}}$	Rodríguez-Pérez et al. 2007
Renormalized						
Chlorophyll	Canopy		Difference Vegetation Index	rDVI	$\frac{R_{880} - R_{673}}{R_{880} + R_{673}}$	Roujean and Breon 1995
Anthocyanins, Chlorophyll	Leaf	Late	Red-Green Ratio Index	RGRl	$\frac{R_{680}}{R_{550}}$	Gamon and Surfus 1999
Relative						
Pigment, Biomass	Chlorophyll, LAI	Leaf, Canopy	Normalized Difference Vegetation Index	rNDVI	$\frac{R_{750} - R_{705}}{R_{750} + R_{705}}$	Carter et al. 1996, Gitelson and Merzlyak 1994
Pigment						
Carotenoids, Chlorophyll a	Leaf	Early	Structure Intensive	SIP1	$\frac{R_{800} - R_{445}}{R_{800} - R_{680}}$	Peñuelas et al. 1995
		Early	Pigment Index	SIP12	$\frac{R_{800} - R_{445}}{R_{800} + R_{445}}$	
Chlorophyll				SR1	$\frac{R_{678}}{R_{880}}$	
			Simple Ratio Index	SR2	$\frac{R_{678}}{R_{1070}}$	

Stress	Temperature		SR3	$\frac{R_{750}}{R_{705}}$	
Water	Late		SR4	$\frac{R_{1070}}{R_{1340}}$	
Pigment	Chlorophyll	Leaf	SRPI	$\frac{R_{430}}{R_{680}}$	Peñuelas et al. 1995
		Early			
		Late	SRW1	$\frac{R_{858}}{R_{1240}}$	
Water	CWC	Canopy	SRW2	$\frac{R_{1350}}{R_{870}}$	Zarco-Tejada and Ustin 2001
		Late			
		Late	SRW3	$\frac{R_{880}}{R_{1265}}$	
Pigment	Chlorophyll	Leaf, Canopy	tCARI	$3 * (R_{700} - R_{670}) - 0.2$	Haboudane et al. 2002
				$* (R_{700} + R_{550})$	
				$* \frac{R_{700}}{R_{670}}$	
		Leaf	Vogelmann Index	$\frac{R_{740}}{R_{720}}$	
			Vogl		



**Supplementary Table 2.** Mann-Whitney U mean separation test of Hyperspectral vegetation indices (HVIs) with significant differences during water stress imposed on July 13<sup>th</sup>, 2018. Differences were detected between stressed (S1 and S2), moderately stressed (M), and well-watered (WW) blocks. Significant p-values are represented as <.001, <.01, and <.05.

TOD	Vegetation Index	Treatment Comparison		p-value	
930	ARI1	S2	WW	< .01	
	ARI2	S2	WW	< .01	
	CAI1	S1	WW	<.001	
		S1	M	< .01	
		S2	WW	<.001	
		S2	M	< .01	
		CAI2	S1	WW	<.001
			S2	WW	<.001
	CAI2	S2	M	< .01	
		WW	M	<.05	
		Crt2	S1	WW	<.001
			S1	M	< .01
	Crt2	S2	WW	<.001	
		S2	M	<.001	
		Crt5	S1	WW	<.001
			S1	M	< .01
	Crt5	S2	WW	<.001	
		S2	M	<.001	
		CRI2	S2	WW	<.05
			S2	M	<.05
	DVI	S1	WW	< .01	
		S2	WW	< .01	
mCARI2	S1	WW	<.001		
	S1	M	<.05		

---

	S2	WW	< .01
MSI1	S1	WW	<.05
	S2	WW	< .01
MSI2	S1	WW	<.05
	S2	WW	< .01
mSR1	S1	WW	<.05
	S1	M	<.05
	S2	WW	< .01
	S2	M	< .01
mTVI2	S1	WW	<.05
	S2	WW	< .01
NDII1	S1	WW	<.05
	S2	WW	< .01
NDII2	S1	WW	<.05
	S2	WW	< .01
NDII3	S1	WW	<.05
	S2	WW	< .01
NDLI	S1	WW	<.05
	S2	WW	<.05
NDWI2	S1	WW	<.05
	S2	WW	<.01
NDWI3	S1	WW	<.01
	S2	WW	<.001
NDWI5	S1	WW	<.05
	S2	WW	<.05
NDWI6	S1	WW	<.05
	S2	WW	<.05
	WW	M	<.05

---

NPCI	S1	WW	<.001
	S1	M	<.001
	S2	WW	<.001
	S2	M	<.001
NPQI	S1	WW	<.001
	S1	M	<.001
	S2	WW	<.001
	S2	M	<.001
PRI1	S2	WW	<.05
PRI2	S2	WW	<.05
PRI3	S2	WW	<.05
PRI4	S2	WW	<.05
PSRI	S1	WW	<.001
	S1	M	<.001
	S2	WW	<.001
	S2	M	<.001
PSSRc	S2	WW	<.05
	S2	M	<.05
RBI	S1	WW	<.001
	S1	M	<.05
	S2	WW	<.001
	S2	M	<.01
SIPI1	S1	WW	<.001
	S1	M	<.001
	S2	WW	<.001
	S2	M	<.001
SIPI2	S1	WW	<.05
	S1	M	<.05



---

		S2	WW	<.01
		S2	M	<.01
	SR4	S2	WW	<.05
	SRPI	S1	WW	<.001
		S1	M	<.01
		S2	WW	<.001
		S2	M	<.001
	SRWI2	S2	WW	<.05
	WBI	S2	WW	<.05
	WI1	S1	WW	<.001
		S2	WW	<.001
		S2	M	<.05
		WW	M	<.01
	WI2	S1	WW	<.05
		S2	WW	<.05
	WI3	S1	WW	<.05
		S2	WW	<.05
1130	ACI	S1	S2	<.05
		S1	WW	<.01
		S1	M	<.05
	ARI1	S1	WW	<.001
		S1	M	<.001
		S2	WW	<.01
		S2	M	<.05
	ARI2	S1	WW	<.001
		S1	M	<.001
		S2	WW	<.01
		S2	M	<.01

---

CAI1	S2	WW	<.05
CARI	S1	WW	<.05
	S1	M	<.05
CIgreen	S1	S2	<.01
	S1	WW	<.01
	S1	M	<.01
CIred_edge	S1	WW	<.05
	WW	M	<.05
Crt1	S1	S2	<.05
	S1	WW	<.01
	S1	M	<.01
Crt2	S1	WW	<.001
	S1	M	<.001
	S2	WW	<.001
	S2	M	<.001
Crt3	S1	WW	<.05
	S1	M	<.05
Crt4	S1	S2	<.05
	S1	WW	<.01
	S1	M	<.01
Crt5	S1	WW	<.001
	S1	M	<.001
	S2	WW	<.001
	S2	M	<.001
Crt6	S1	WW	<.01
	S1	M	<.05
CRI1	S2	M	<.05
CRI2	S1	M	<.05

---

	S2	WW	<.01
	S2	M	<.01
CUR	S1	M	<.05
DattsCI	S1	WW	<.05
	S1	M	<.05
DVI	S1	S2	<.01
	S1	M	<.05
EVI	S1	S2	<.05
	S1	WW	<.05
GMI1	S1	S2	<.05
	S1	WW	<.01
	S1	M	<.01
GMI2	S1	S2	<.05
	S1	WW	<.01
	S1	M	<.01
mARI	S1	S2	<.05
	S2	M	<.01
mCARI1	S1	WW	<.05
	S1	M	<.05
mCARI2	S1	M	<.05
mNDVI	S1	WW	<.01
	S1	M	<.01
mSR1	S1	S2	<.05
	S1	M	<.05
	S2	WW	<.01
	S2	M	<.001
mSR2	S1	S2	<.05
	S1	WW	<.01

---

	S1	M	<.05
MTCI	S1	WW	<.01
	S1	M	<.05
mTVI1	S1	S2	<.05
	S1	M	<.01
mTVI2	S1	S2	<.01
	S1	M	<.01
NDVI1	S1	S2	<.05
	S1	WW	<.01
NDVI2	S1	S2	<.05
	S1	WW	<.01
	S1	M	<.05
NDVI3	S1	S2	<.05
	S1	WW	<.01
	S1	M	<.05
NDVI4	S1	S2	<.05
	S1	WW	<.01
NDVI5	S1	S2	<.05
	S1	WW	<.01
NDVI6	S1	S2	<.05
	S1	WW	<.01
NDWI1	S1	M	<.01
NDWI4	S1	M	<.01
NDWI5	S2	M	<.01
NDWI6	S1	M	<.05
	S2	M	<.01
NPCI	S1	S2	<.01
	S1	WW	<.001

---

	S1	M	<.001
	S2	WW	<.001
	S2	M	<.001
NPQI	S1	WW	<.001
	S1	M	<.001
	S2	WW	<.001
	S2	M	<.001
PRI1	S1	WW	<.05
	S1	M	<.01
PRI2	S1	WW	<.05
	S1	M	<.05
PRI3	S1	WW	<.01
	S1	M	<.01
PRI4	S1	WW	<.01
	S1	M	<.01
PSNDa	S1	S2	<.05
	S1	WW	<.01
	S1	M	<.05
PSNDb	S1	S2	<.05
	S1	WW	<.01
	S1	M	<.05
PSNDc	S1	S2	<.05
	S2	M	<.05
PSRI	S1	S2	<.05
	S1	WW	<.001
	S1	M	<.001
	S2	WW	<.001
	S2	M	<.001

---

PSSRa	S1	S2	<.05
	S1	WW	<.01
	S1	M	<.05
PSSRb	S1	S2	<.05
	S1	WW	<.01
	S1	M	<.05
PSSRc	S1	S2	<.05
	S2	WW	<.05
	S2	M	<.01
RARSb	S1	WW	<.01
RARSc	S1	S2	<.05
	S2	M	<.05
RBI	S1	WW	<.001
	S1	M	<.001
	S2	WW	<.001
	S2	M	<.001
rDVI	S1	S2	<.05
	S1	WW	<.01
rNDVI	S1	WW	<.01
	S1	M	<.01
SIP11	S1	S2	<.01
	S1	WW	<.001
	S1	M	<.001
	S2	WW	<.001
	S2	M	<.001
SIP12	S1	S2	<.05
	S1	M	<.05
	S2	WW	<.01

---

	S2	M	<.001
SR1	S1	S2	<.05
	S1	WW	<.01
SR2	S1	S2	<.05
	S1	WW	<.01
SR3	S1	WW	<.01
	S1	M	<.01
SR4	S2	M	<.05
SRPI	S1	S2	<.01
	S1	WW	<.001
	S1	M	<.001
	S2	WW	<.001
	S2	M	<.001
SRWI1	S1	M	<.01
SRWI3	S1	M	<.01
tCARI	S1	WW	<.05
	S1	M	<.05
Vog1	S1	WW	<.01
	S1	M	<.05
Vog2	S1	WW	<.01
	S1	M	<.05
Vog3	S1	WW	<.01
	S1	M	<.05
WI1	S1	M	<.05
	S2	M	<.05
WI2	S2	M	<.01
WI3	S2	M	<.01
1600 CAI1	WW	M	<.01

---

CAI2	WW	M	<.05
CARI	S1	WW	<.01
	S1	M	<.01
Crt2	S1	WW	<.001
	S1	M	<.001
	S2	WW	<.05
	S2	M	<.05
Crt3	S1	WW	<.01
	S1	M	<.01
	S2	M	<.05
Crt5	S1	WW	<.001
	S1	M	<.001
	S2	WW	<.01
	S2	M	<.01
CRI1	S1	WW	<.05
	S1	M	<.05
CRI2	S1	M	<.05
CUR	S1	WW	<.01
	S1	M	<.01
	S2	WW	<.05
	S2	M	<.05
DVI	S1	WW	<.05
	S1	M	<.001
	S2	M	<.01
mCARI1	S1	WW	<.01
	S1	M	<.01
mCARI2	S1	WW	<.01
	S1	M	<.001



---

	S2	WW	<.05
	S2	M	<.001
MSI1	S1	WW	<.001
	S1	M	<.001
	S2	WW	<.001
	S2	M	<.001
	WW	M	<.05
MSI2	S1	WW	<.001
	S1	M	<.001
	S2	WW	<.001
	S2	M	<.001
	WW	M	<.05
mSR1	S1	WW	<.01
	S1	M	<.01
mTVI1	S1	WW	<.05
	S1	M	<.05
mTVI2	S1	WW	<.01
	S1	M	<.001
	S2	M	<.01
NDII1	S1	WW	<.001
	S1	M	<.001
	S2	WW	<.001
	S2	M	<.001
	WW	M	<.05
NDII2	S1	WW	<.001
	S1	M	<.001
	S2	WW	<.001
	S2	M	<.001

---

	WW	M	<.05
NDII3	S1	WW	<.001
	S1	M	<.001
	S2	WW	<.001
	S2	M	<.001
	WW	M	<.05
NDLI	S1	WW	<.001
	S1	M	<.001
	S2	WW	<.001
	S2	M	<.001
NDNI	S1	S2	<.05
	S1	WW	<.001
	S1	M	<.001
	S2	WW	<.001
	S2	M	<.001
NDVI1	S1	WW	<.05
NDVI2	S1	WW	<.05
NDVI5	S1	WW	<.05
NDVI6	S1	WW	<.05
NDWI1	S1	WW	<.001
	S1	M	<.001
	S2	WW	<.001
	S2	M	<.001
NDWI2	S1	WW	<.001
	S1	M	<.001
	S2	WW	<.001
	S2	M	<.001
	WW	M	<.05

NDWI3	S1	WW	<.01
	S1	M	<.001
	S2	M	<.001
	WW	M	<.05
NDWI4	S1	WW	<.001
	S1	M	<.001
	S2	WW	<.001
	S2	M	<.001
NDWI5	S1	S2	<.05
	S1	WW	<.001
	S1	M	<.001
	S2	WW	<.001
	S2	M	<.001
	WW	M	<.05
NDWI6	S1	S2	<.05
	S1	WW	<.001
	S1	M	<.001
	S2	WW	<.001
	S2	M	<.001
	WW	M	<.05
NPCI	S1	WW	<.01
	S1	M	<.05
NPQI	S1	WW	<.01
	S2	WW	<.05
PRI1	S1	WW	<.001
	S1	M	<.01
	S2	WW	<.05
	S2	M	<.05

---

PRI2	S1	WW	<.001
	S1	M	<.01
	S2	WW	<.01
	S2	M	<.05
PRI3	S1	WW	<.001
	S1	M	<.05
	S2	WW	<.05
PRI4	S1	WW	<.01
	S2	WW	<.05
PSNDa	S1	WW	<.05
PSNDc	S1	WW	<.05
PSSRa	S1	WW	<.05
PSSRc	S1	WW	<.05
	S1	M	<.05
RARSa	S1	S2	<.05
	S1	WW	<.01
	S1	M	<.001
	S2	M	<.05
RARSb	S1	WW	<.05
RARSc	S1	WW	<.05
RBI	S1	WW	<.001
	S1	M	<.001
	S2	WW	<.05
	S2	M	<.05
RGRI	S1	S2	<.05
	S1	WW	<.01
	S1	M	<.001
	S2	M	<.05

---

SIPI2	S1	WW	<.01
	S1	M	<.05
SR1	S1	WW	<.05
SR4	S1	S2	<.05
	S1	WW	<.001
	S1	M	<.001
	S2	WW	<.001
	S2	M	<.001
	WW	M	<.001
SRPI	S1	WW	<.01
	S1	M	<.05
SRWI1	S1	WW	<.001
	S1	M	<.001
	S2	WW	<.001
	S2	M	<.001
SRWI2	S1	S2	<.05
	S1	WW	<.001
	S1	M	<.001
	S2	WW	<.001
	S2	M	<.001
SRWI3	S1	WW	<.001
	S1	M	<.001
	S2	WW	<.001
	S2	M	<.001
tCARI	S1	WW	<.01
	S1	M	<.01
WBI	S1	S2	<.05
	S1	WW	<.001

---

	S1	M	<.001
	S2	WW	<.05
	S2	M	<.001
	WW	M	<.05
WI1	S1	S2	<.05
	S1	WW	<.001
	S1	M	<.001
	S2	WW	<.001
	S2	M	<.001
WI2	S1	S2	<.05
	S1	WW	<.001
	S1	M	<.001
	S2	WW	<.001
	S2	M	<.001
	WW	M	<.05
WI3	S1	S2	<.05
	S1	WW	<.001
	S1	M	<.001
	S2	WW	<.001
	S2	M	<.001
	WW	M	<.05

**Supplementary Table 3.** Fowlkes-Mallows Index (FMI) scores for results of Birch clustering algorithm (threshold=0.01, n=2) of correlations between selected HVIs and stomatal conductance ( $g_{sw}$ ). Selected HVIs are sensitive to these block differences at 930 and/or 1130. Scores range from 0 to 1. Values closer to 1 indicate better separation between clusters.

Conventional stress measure	Index	Time of Day		
		930	1130	1600
$g_{sw}$	CAI1	0.876	0.551	0.487
	Crt2	0.821	0.765	0.734
	NPCI	0.876	0.844	0.676
	PSRI	0.697	0.653	0.660
	RBI	0.688	0.844	0.734
	SIPI1	0.531	0.570	0.750

**Supplementary Table 4.** Fowlkes-Mallows Index (FMI) scores for results of Birch clustering algorithm (threshold=0.01, n=2) of correlations between selected HVIs and stomatal conductance ( $g_{sw}$ ). Selected HVIs are sensitive to these block differences at 1600.

Conventional stress measure	Index	Time of Day		
		930	1130	1600
$\Psi_{leaf}$	CUR	0.491	0.570	0.750
	MSI1	0.531	0.570	0.750
	NDII1	0.491	0.570	0.750
	SRWI1	0.531	0.570	0.750
	WBI	0.531	0.570	0.750
	WI2	0.491	0.602	1.000

## Figures

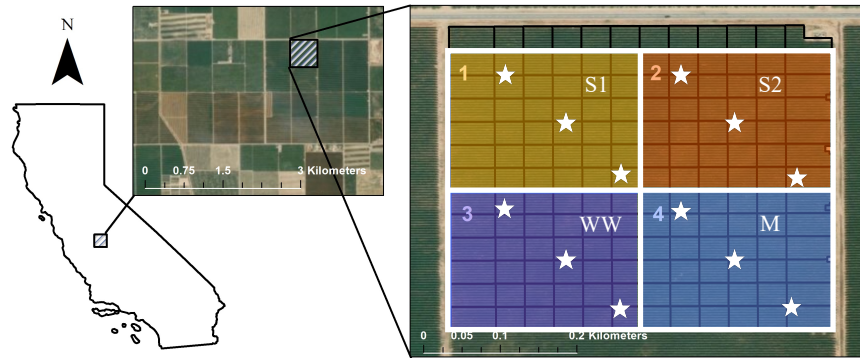


**Figure 1.** Ripperdan 720 (RIP720) experimental vineyard in Madera, CA, 25 km west of Fresno, CA. The vineyard is 16 hectares, divided evenly into four blocks. Blocks are named based on irrigation treatment. Blocks are well-watered (purple), mildly stressed (blue), and stressed (yellow and orange). The northwestern block (yellow) is referred to as S1 and the northeastern block (orange) is referred to as S2. Three data collection locations (★) were located in each block and a flux tower was located in the southeastern corner of each block. Collections took place on June 19<sup>th</sup>, July 13<sup>th</sup>, and August 6<sup>th</sup>, 2018.

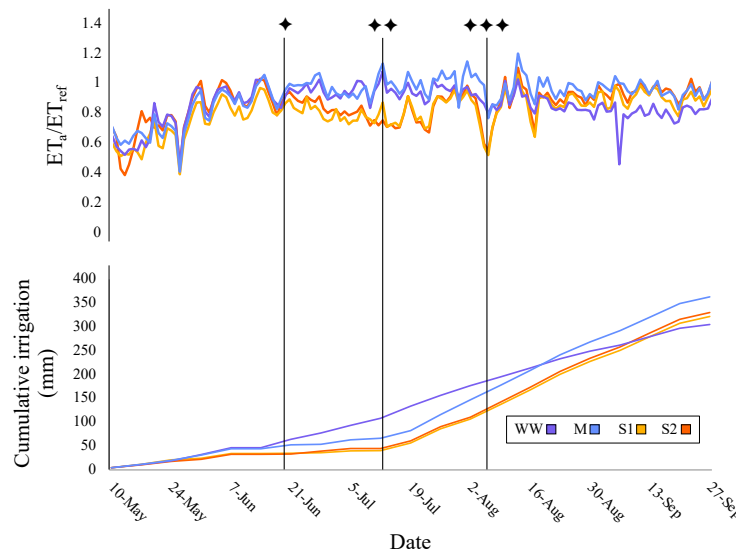


**Figure 2.**  $ET_a/ET_{ref}$  and cumulative irrigation inputs to Ripperdan 720 vineyard in Madera, CA from 17-May to 27-September, 2018. Irrigation was applied to blocks well-watered (purple), mildly stressed (blue), and stressed (yellow and orange). Data collection times are shown as vertical lines. Data were collected on June 19<sup>th</sup> (◆), July 13<sup>th</sup> (◆◆), and August 6<sup>th</sup> (◆◆◆).



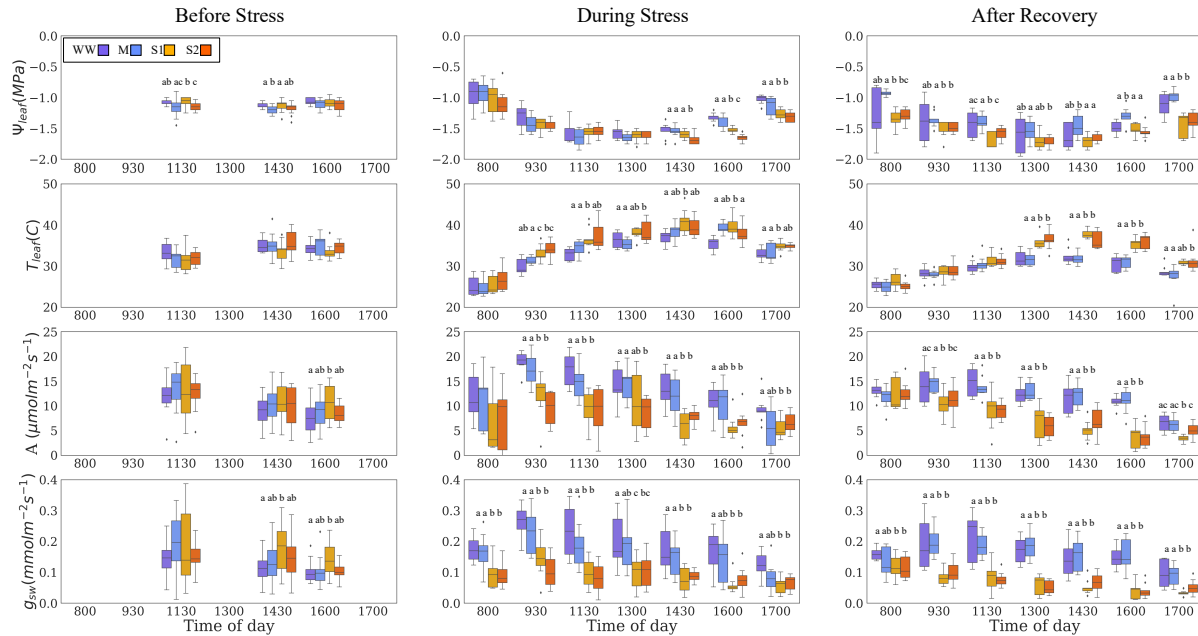


**Figure 3.** Conventional measures of stress detection collected on June 19<sup>th</sup> (“Before Stress”), July 13<sup>th</sup> (“During Stress”), and August 6<sup>th</sup> (“After Recovery”) in Ripperdan 720 vineyard in 2018. Measures include leaf water potential ( $\Psi_{leaf}$ ), leaf temperature ( $T_{leaf}$ ), net assimilation ( $A$ ), and stomatal conductance ( $g_{sw}$ ). Block treatments are well-watered (WW), mildly stressed (M), and stressed (S1, S2). Measurements were collected throughout the day during each collection day. On July 13<sup>th</sup> and August 6<sup>th</sup>, intensive observational periods (IOP) maximized the number of collection time points to capture differences due to the water stress and recovery phase. Significant differences based on Mann-Whitney U mean separation test between blocks at each time point are presented using different lowercase letters above the block treatment. Lowercase letters do not express differences between collection time points.

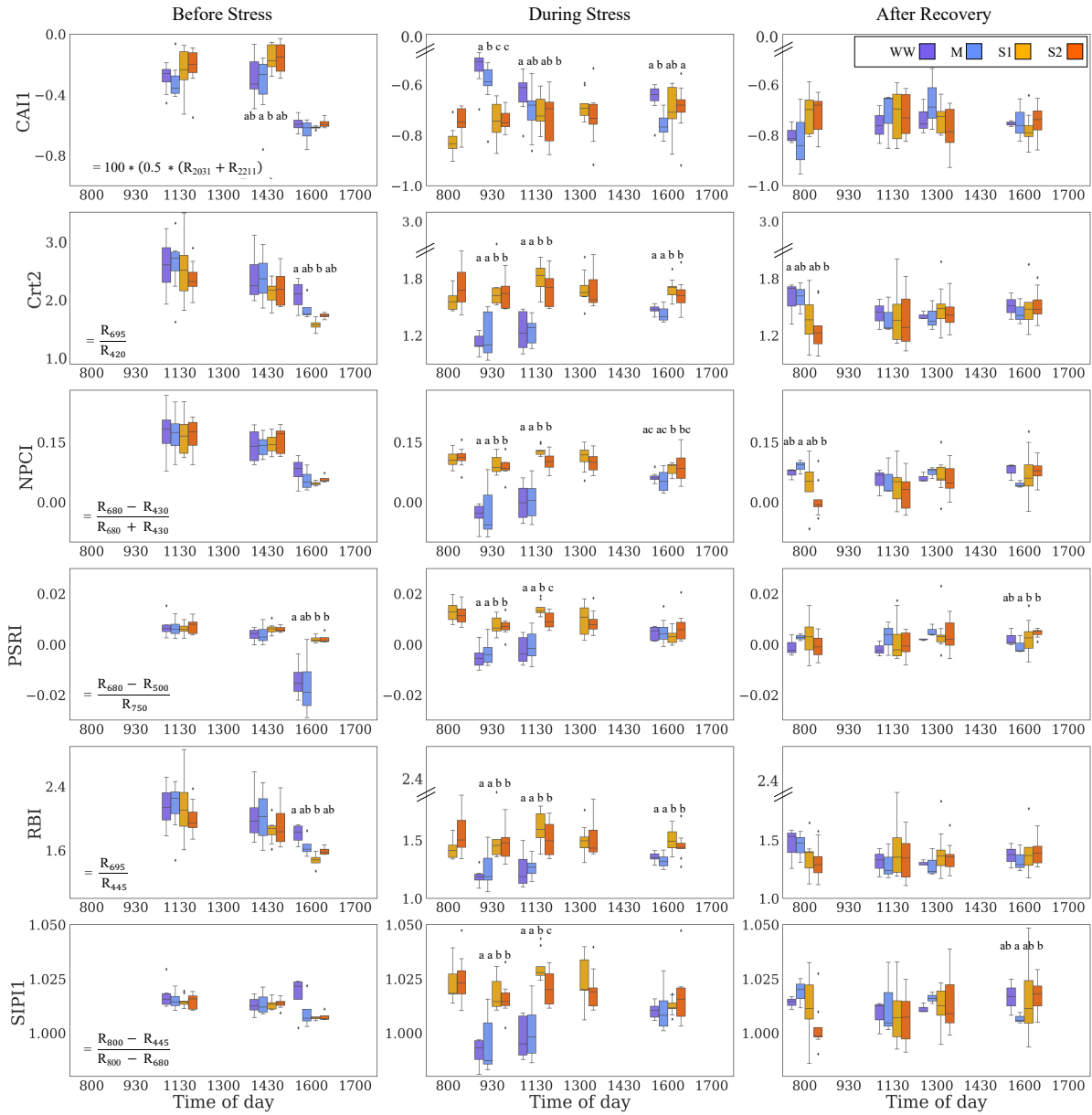


**Figure 4.** Selected hyperspectral vegetation indices (HVIs), and their formulas, showing differences between stressed (S1 and S2), well-watered (WW), and mildly stressed (M) blocks earlier in the day. HVIs were calculated for hyperspectral measurements collected on June 19<sup>th</sup> (“Before Stress”), July 13<sup>th</sup> (“During Stress”), and August 6<sup>th</sup> (“After Recovery”) in Ripperdan 720 vineyard in 2018. Significant differences based on Mann-Whitney U mean separation test between blocks at each time point are presented using different lowercase letters above the block treatment. Lowercase letters do not express differences between collection time points.

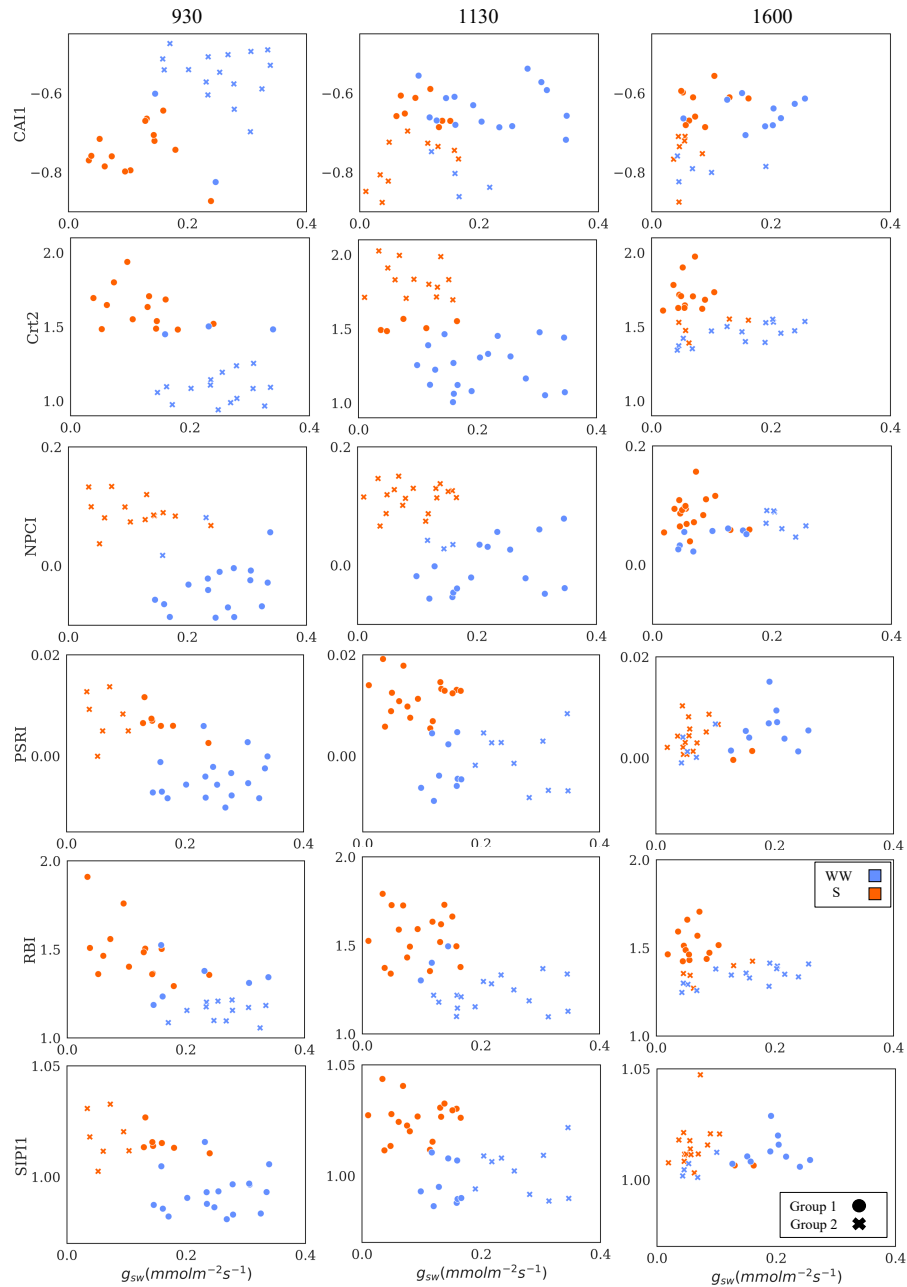


**Figure 5.** Cluster results between selected hyperspectral vegetation indices (HVIs) and stomatal conductance ( $g_{sw}$ ). Data collected from mildly and well-watered blocks were combined as “well-watered” (WW; blue). Data from the two “stressed” (S; orange) blocks were combined. Cluster results were evaluated using Birch (Balanced Iterative Reducing and Clustering using Hierarchies) clustering algorithm (threshold=0.01, n=2). Resulting groups (●, x) are assigned based on the clustering algorithm and have no relationship to treatment conditions.

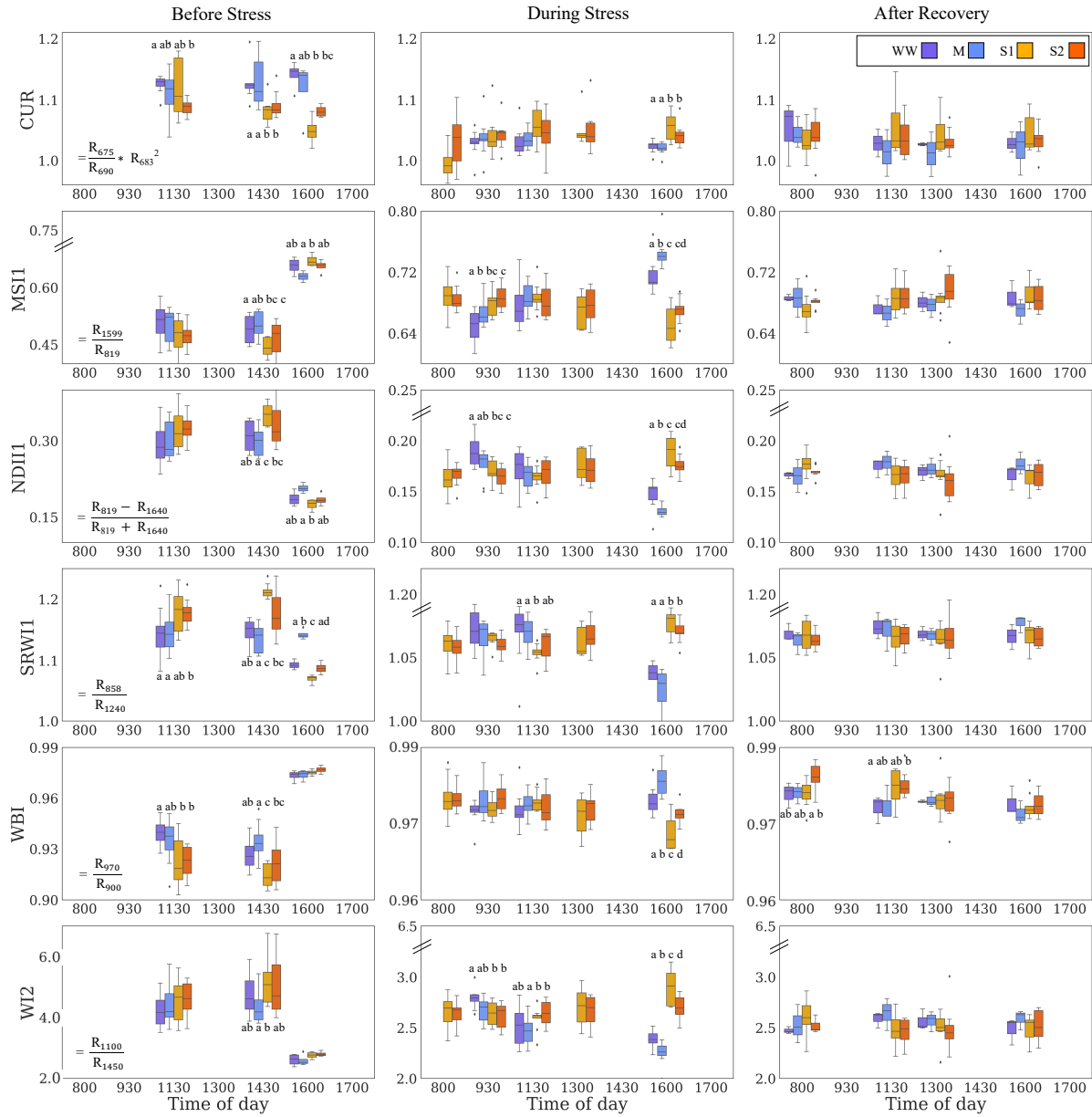


**Figure 6.** Selected hyperspectral vegetation indices (HVIs), and their formulas, showing differences between stressed (S1 and S2), well-watered (WW), and mildly stressed (M) blocks later in the day. HVIs were calculated for hyperspectral measurements collected on June 19<sup>th</sup> (“Before Stress”), July 13<sup>th</sup> (“During Stress”), and August 6<sup>th</sup> (“After Recovery”) in Ripperdan 720 vineyard in 2018. Significant differences based on Mann-Whitney U mean separation test between blocks at each time point are presented using different lowercase letters above the block treatment. Lowercase letters do not express differences between collection time points.

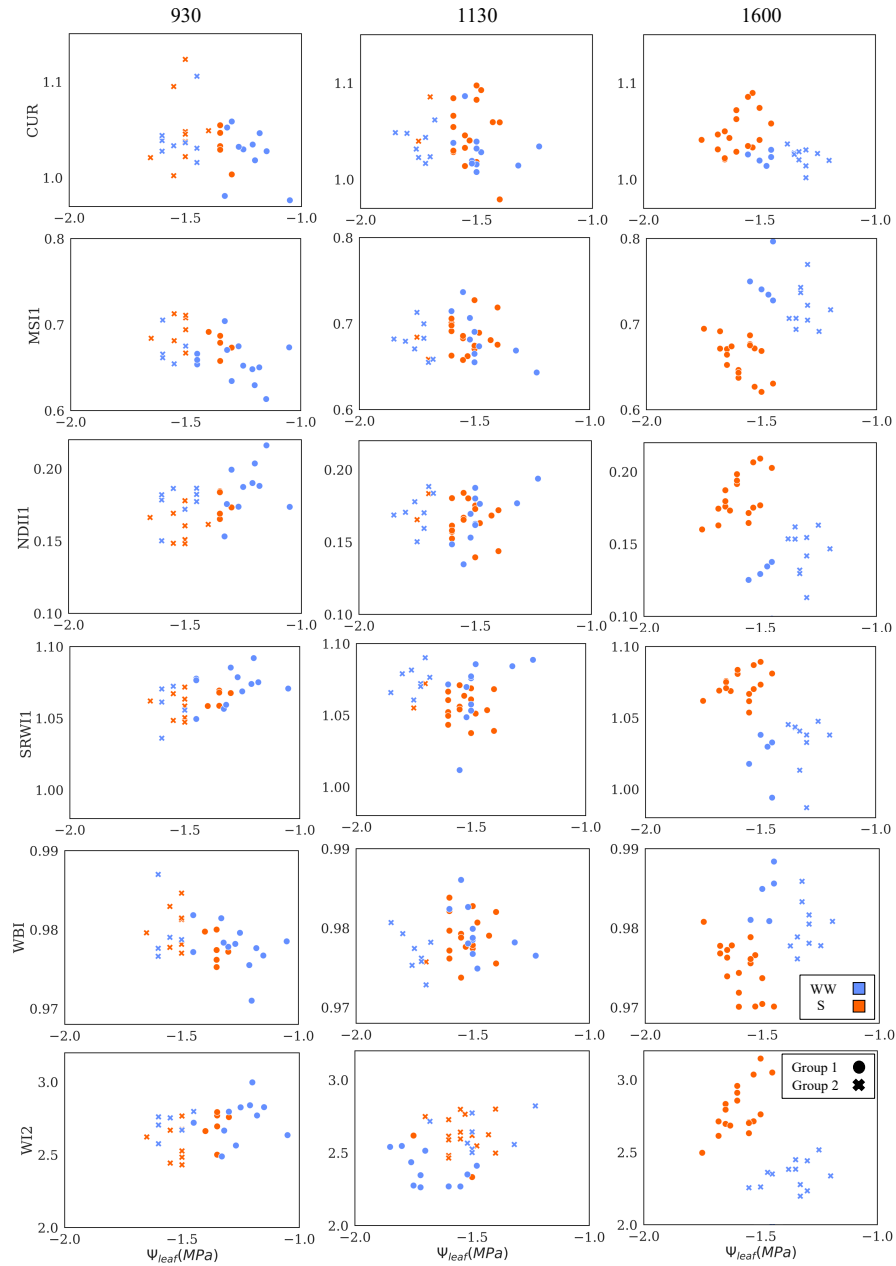
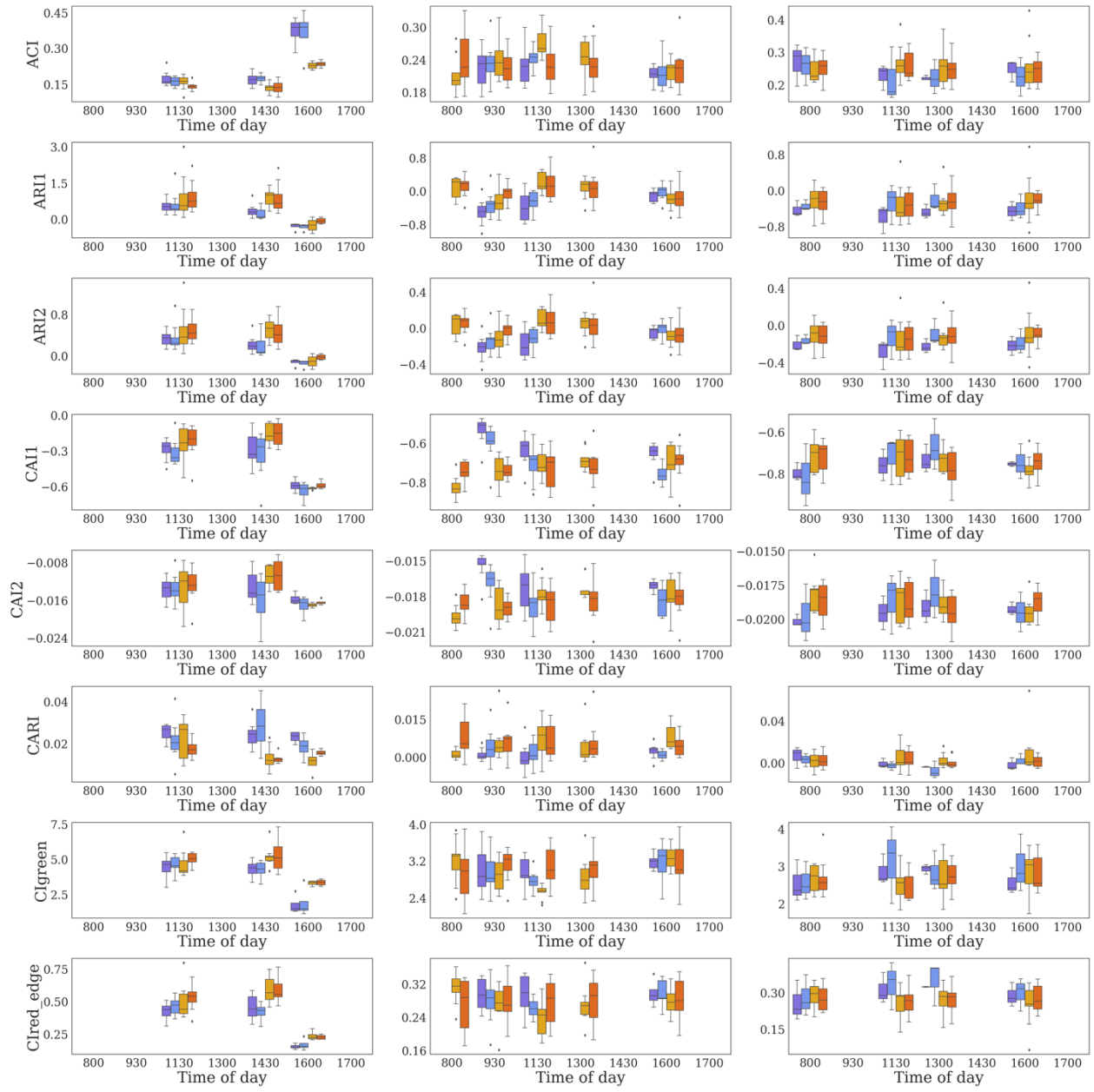
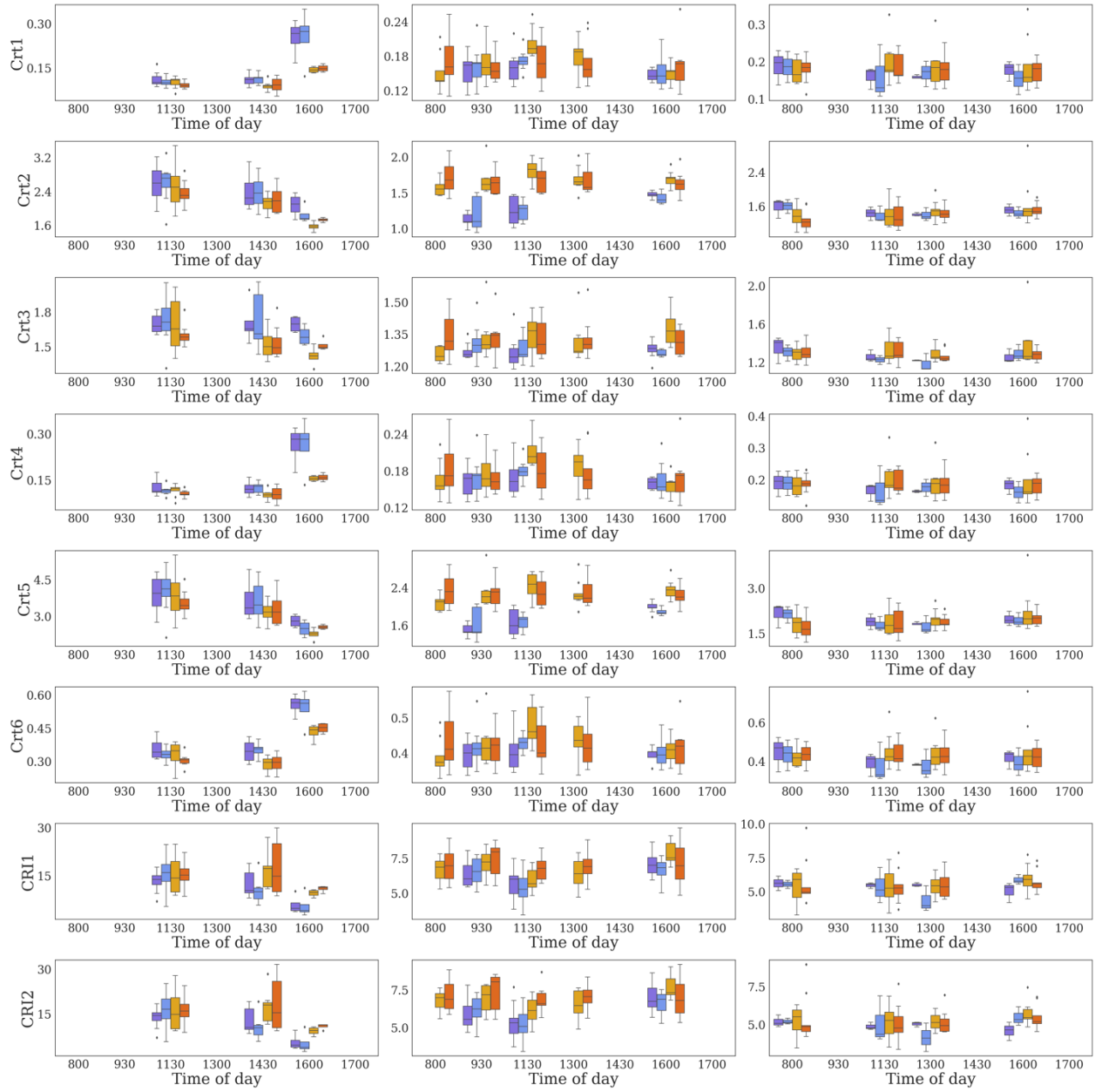


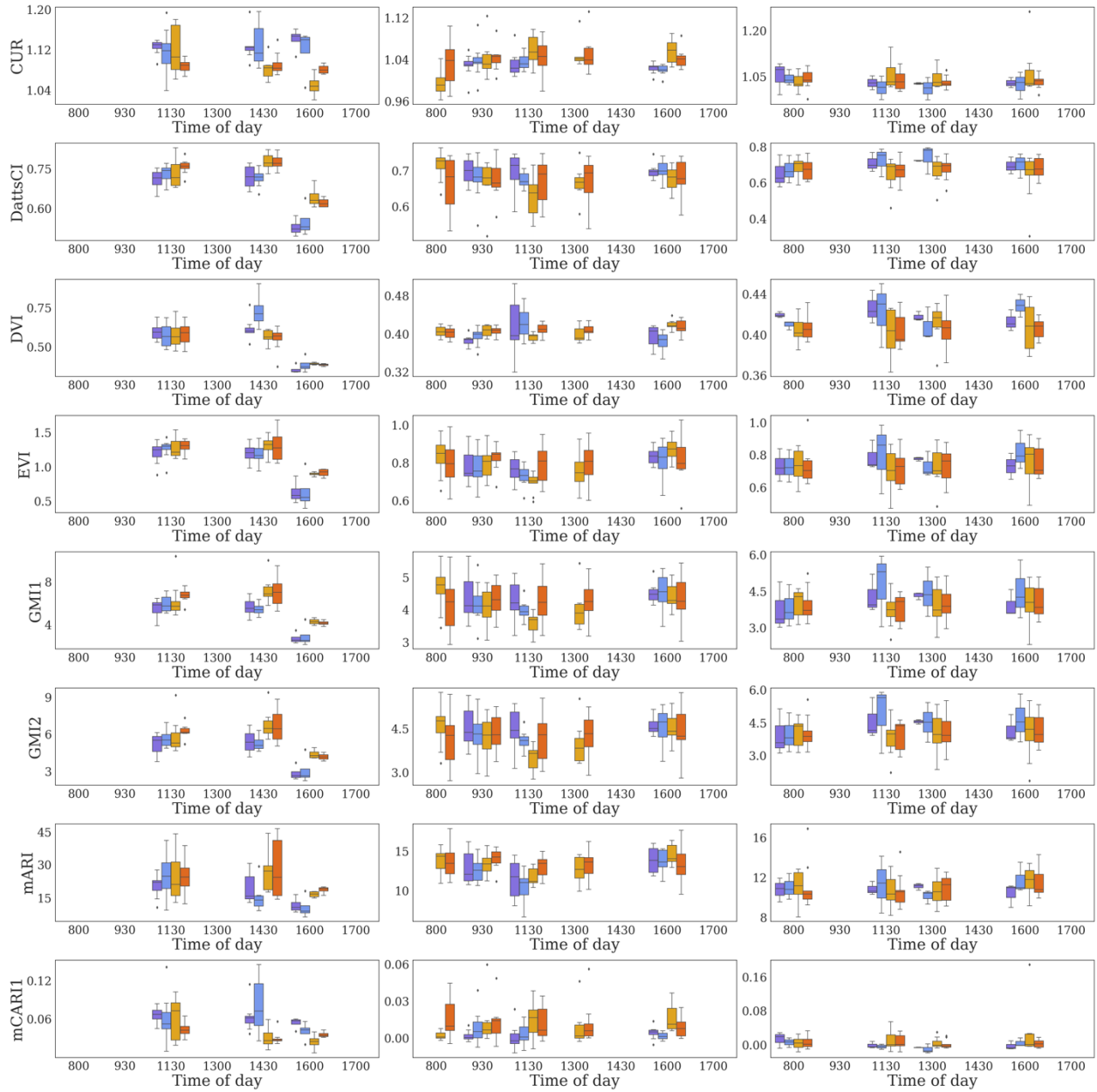
**Figure 7.** Cluster results between selected hyperspectral vegetation indices (HVIs) and leaf water potential ( $\Psi_{leaf}$ ). Data collected from mildly and well-watered blocks were combined as “well-watered” (WW) blocks and “stressed” (S) block data were combined. Cluster results were evaluated using Birch (Balanced Iterative Reducing and Clustering using Hierarchies) clustering algorithm (threshold=0.01, n=2). Resulting groups (●, ×) are assigned based on the clustering algorithm and have no relationship to treatment conditions.



**Supplementary Figure 1.** 88 hyperspectral vegetation indices (HVIs) of stressed (S1 and S2) versus well-watered (WW) and mildly stressed (M) blocks. HVIs were calculated for hyperspectral measurements collected on June 19<sup>th</sup> (“Before Stress”), July 13<sup>th</sup> (“During Stress”), and August 6<sup>th</sup> (“After Recovery”) in Ripperdan 720 vineyard in 2018. Significant differences based on Mann-Whitney U mean separation test between blocks at each time point are presented using different lowercase letters above the block treatment. Lowercase letters do not express differences between collection time points.

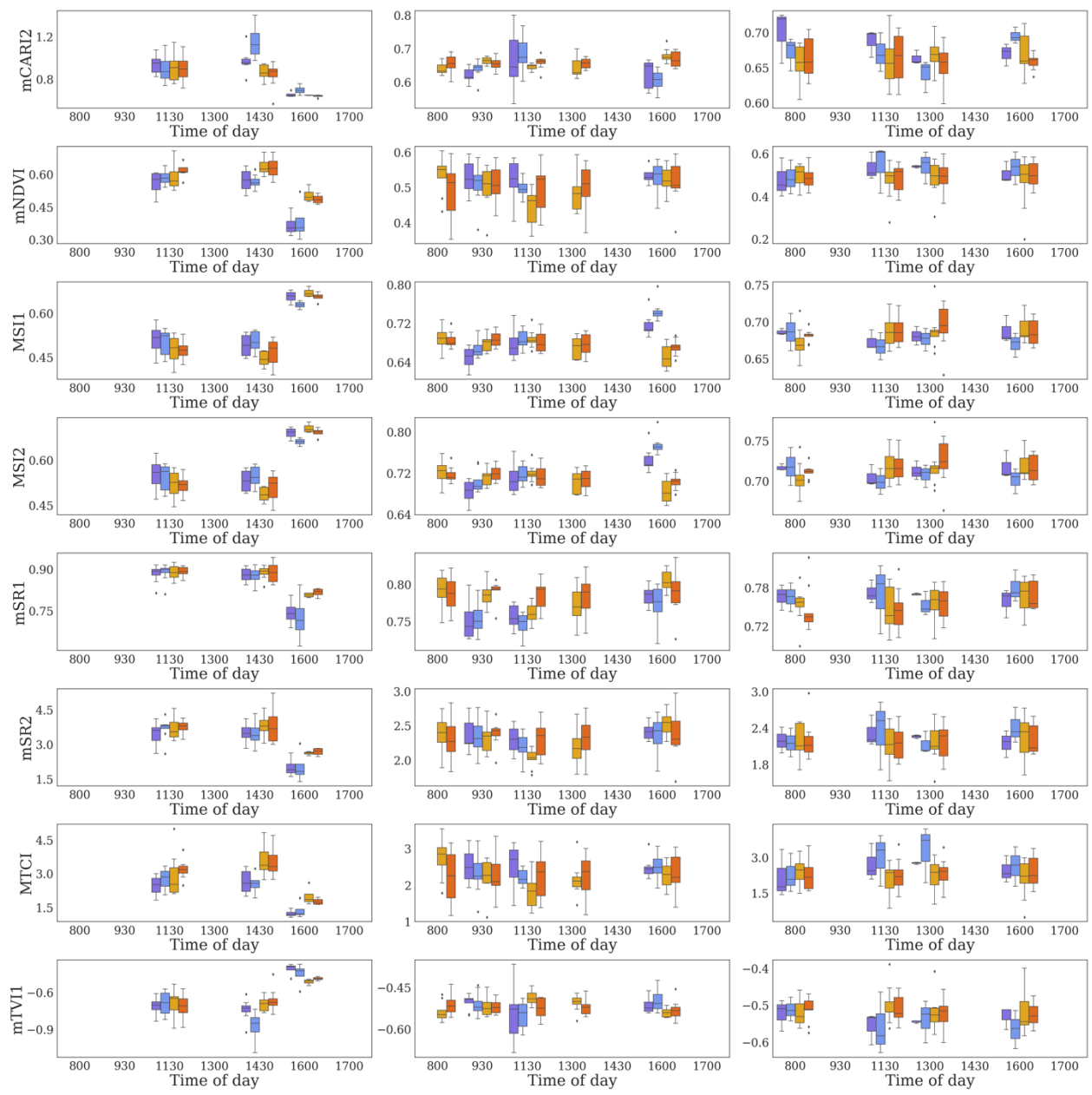


**Supplementary Figure 1 (cont'd).**

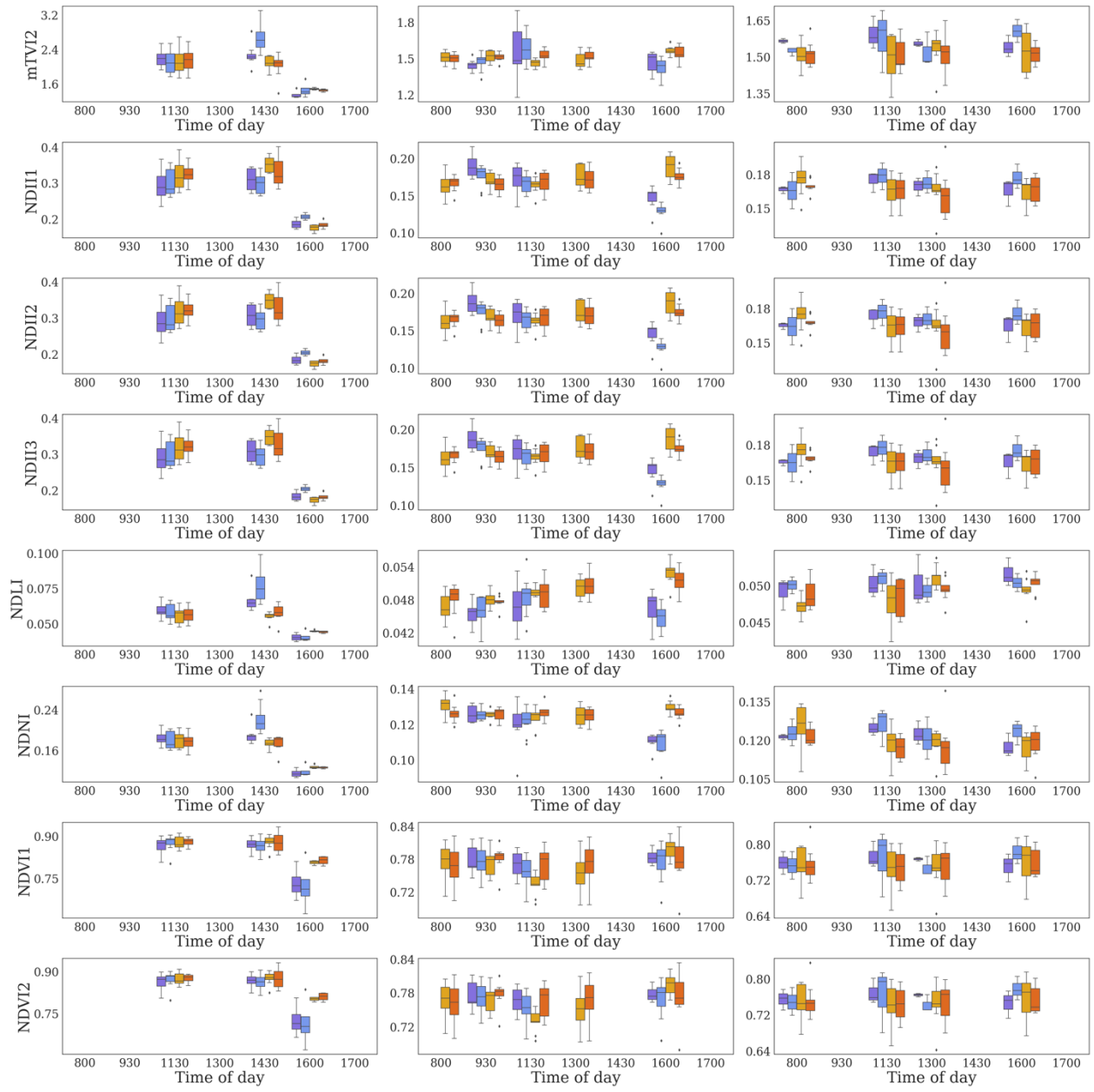


**Supplementary Figure 1 (cont'd).**

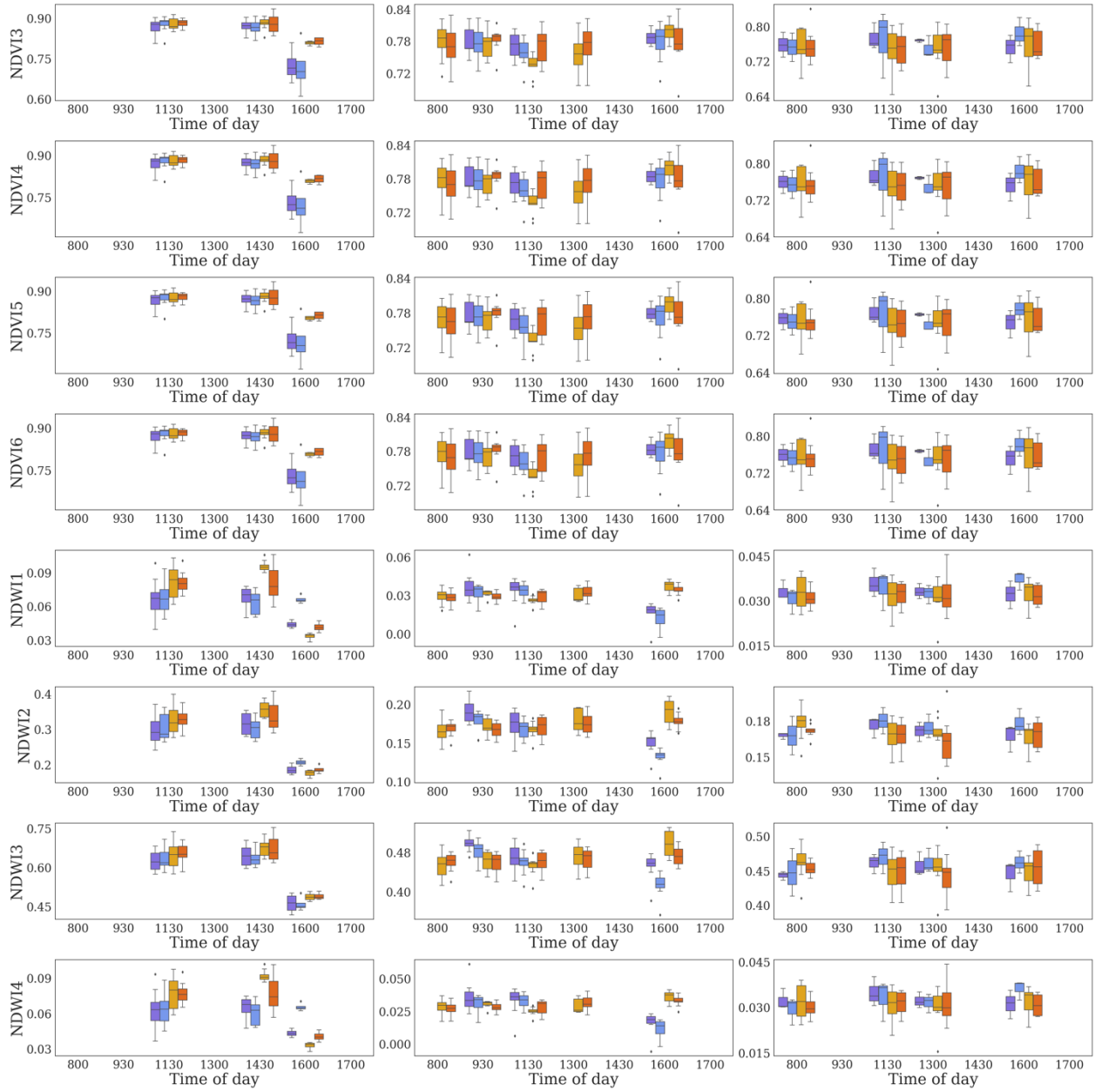




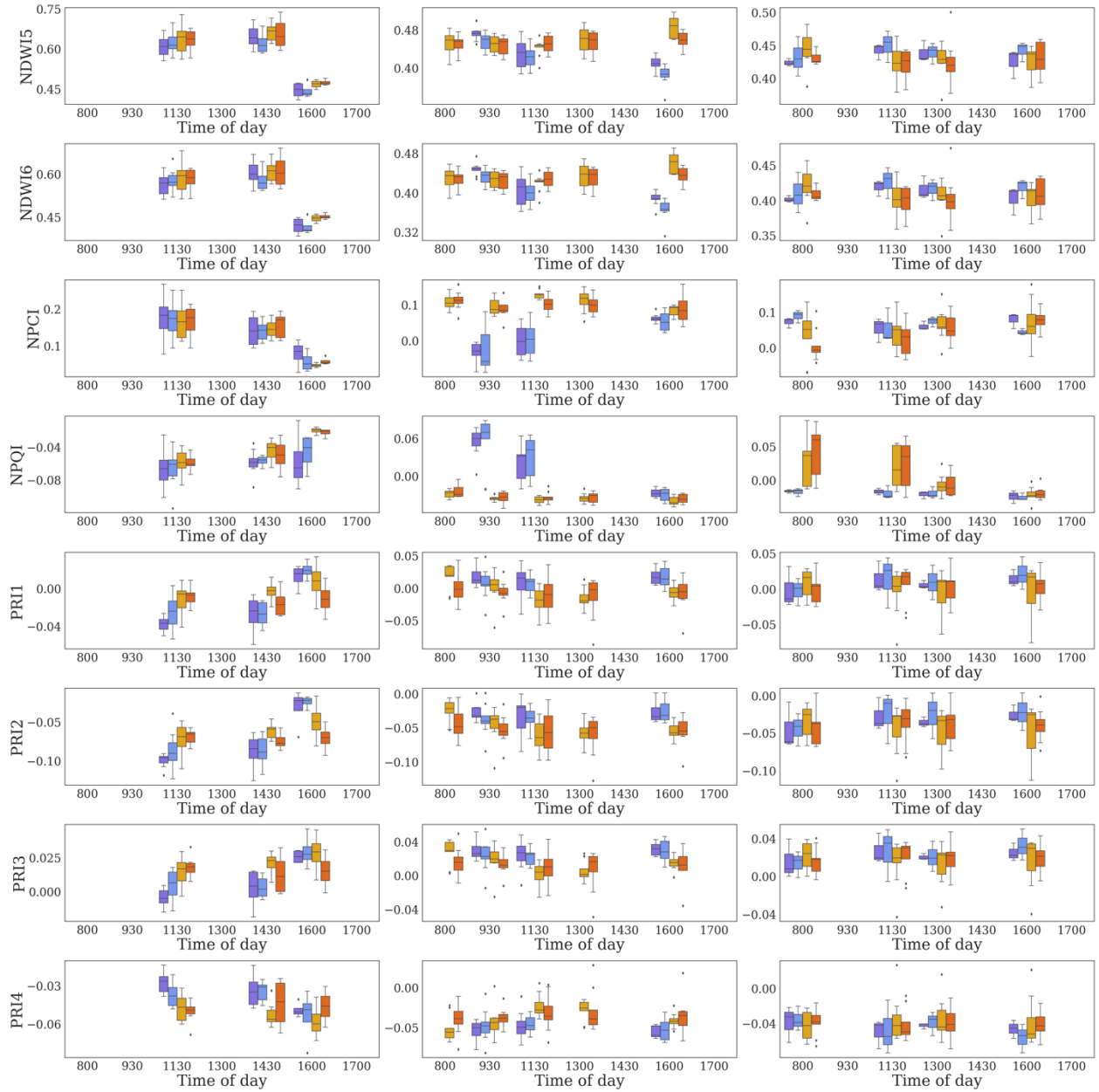
**Supplementary Figure 1 (cont'd).**



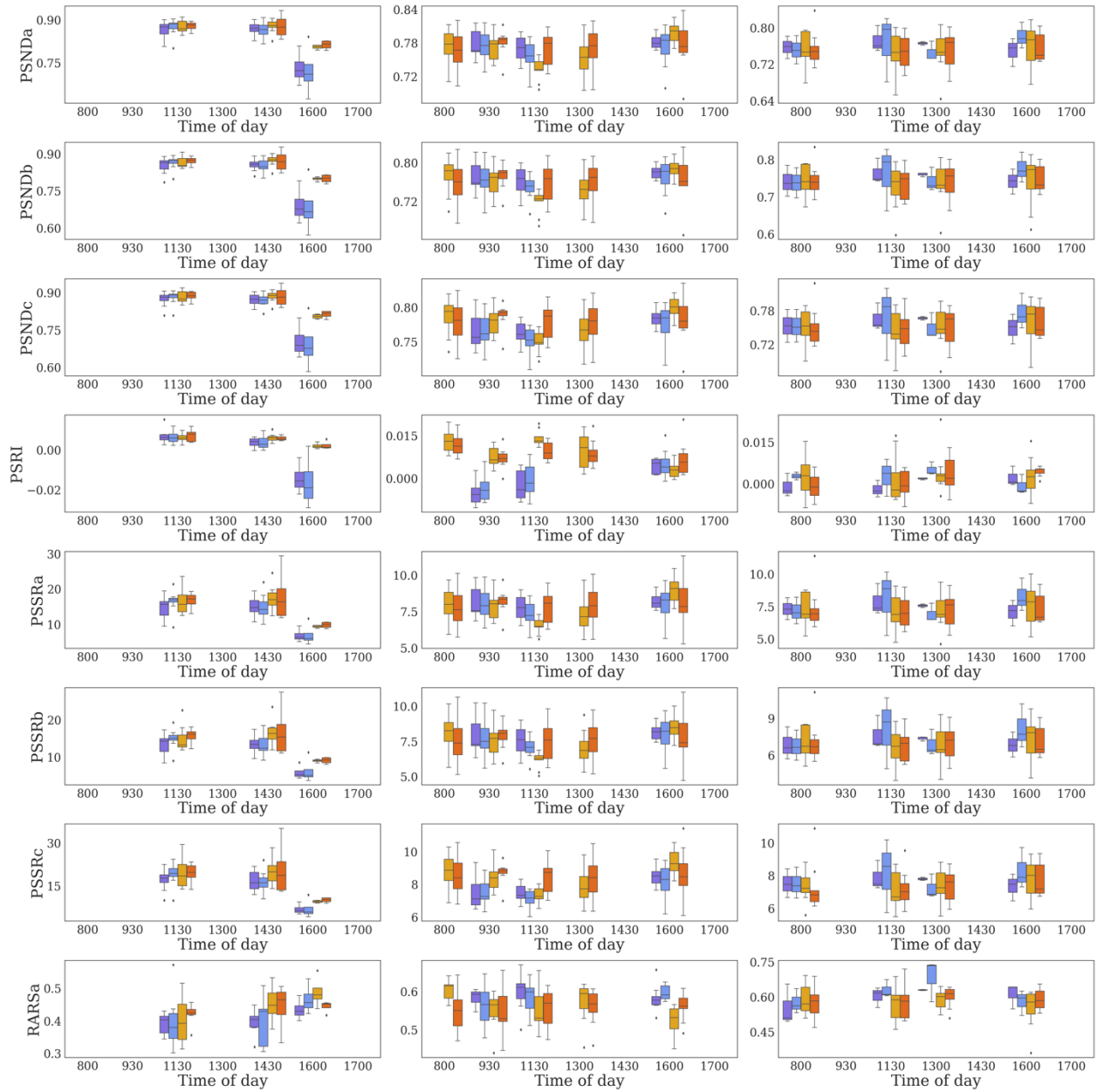
**Supplementary Figure 1 (cont'd).**



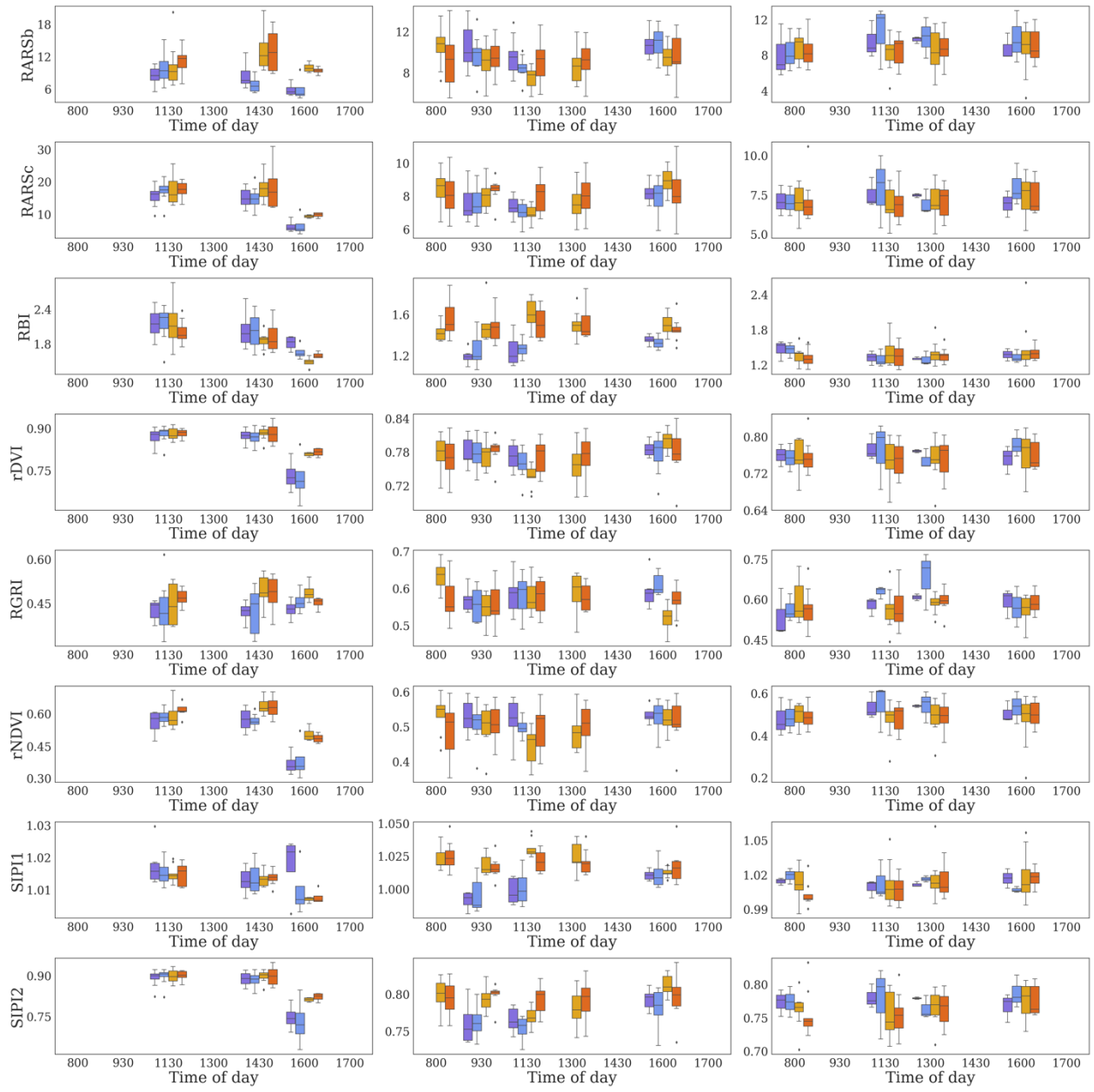
**Supplementary Figure 1 (cont'd).**



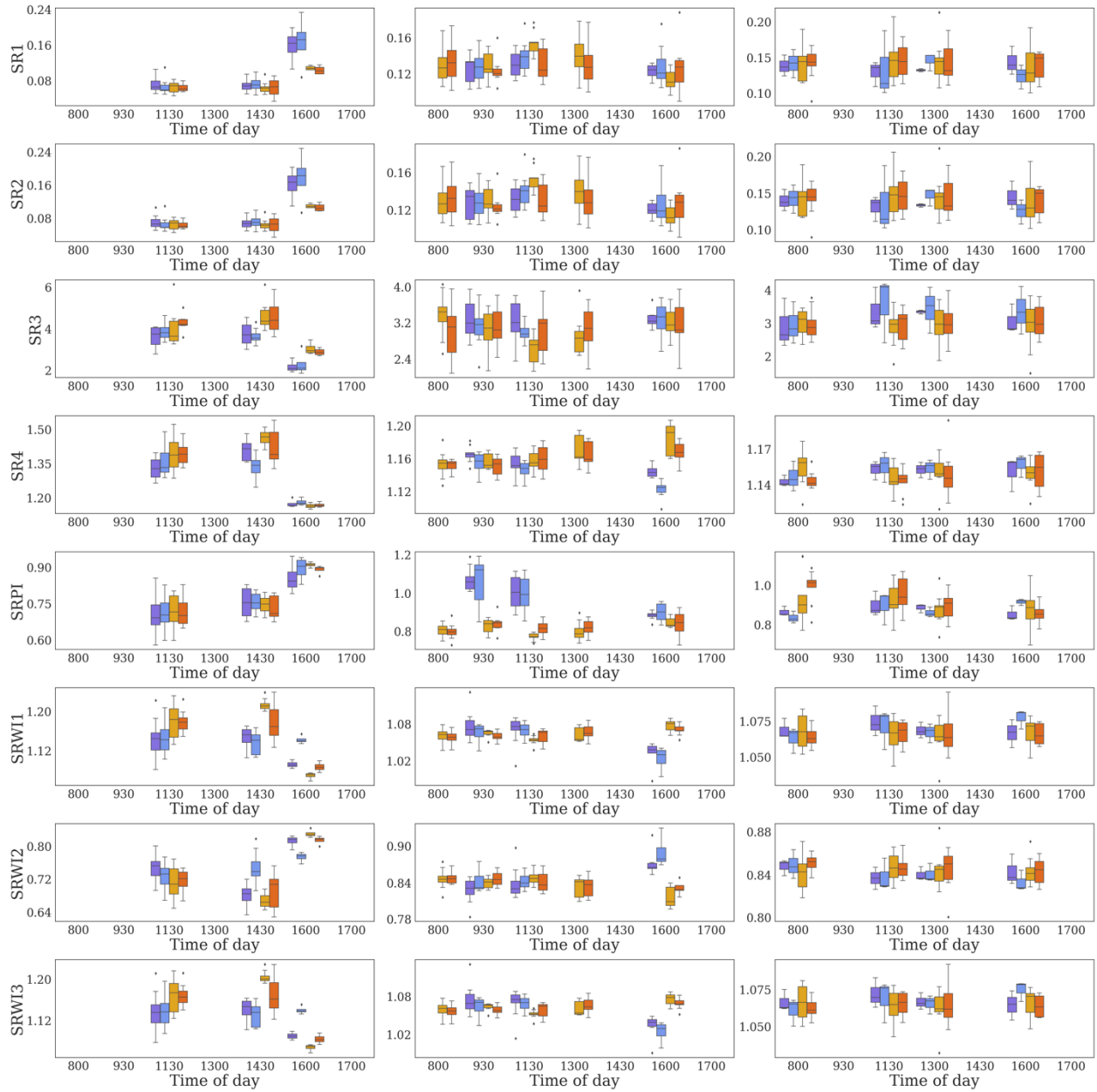
**Supplementary Figure 1 (cont'd).**



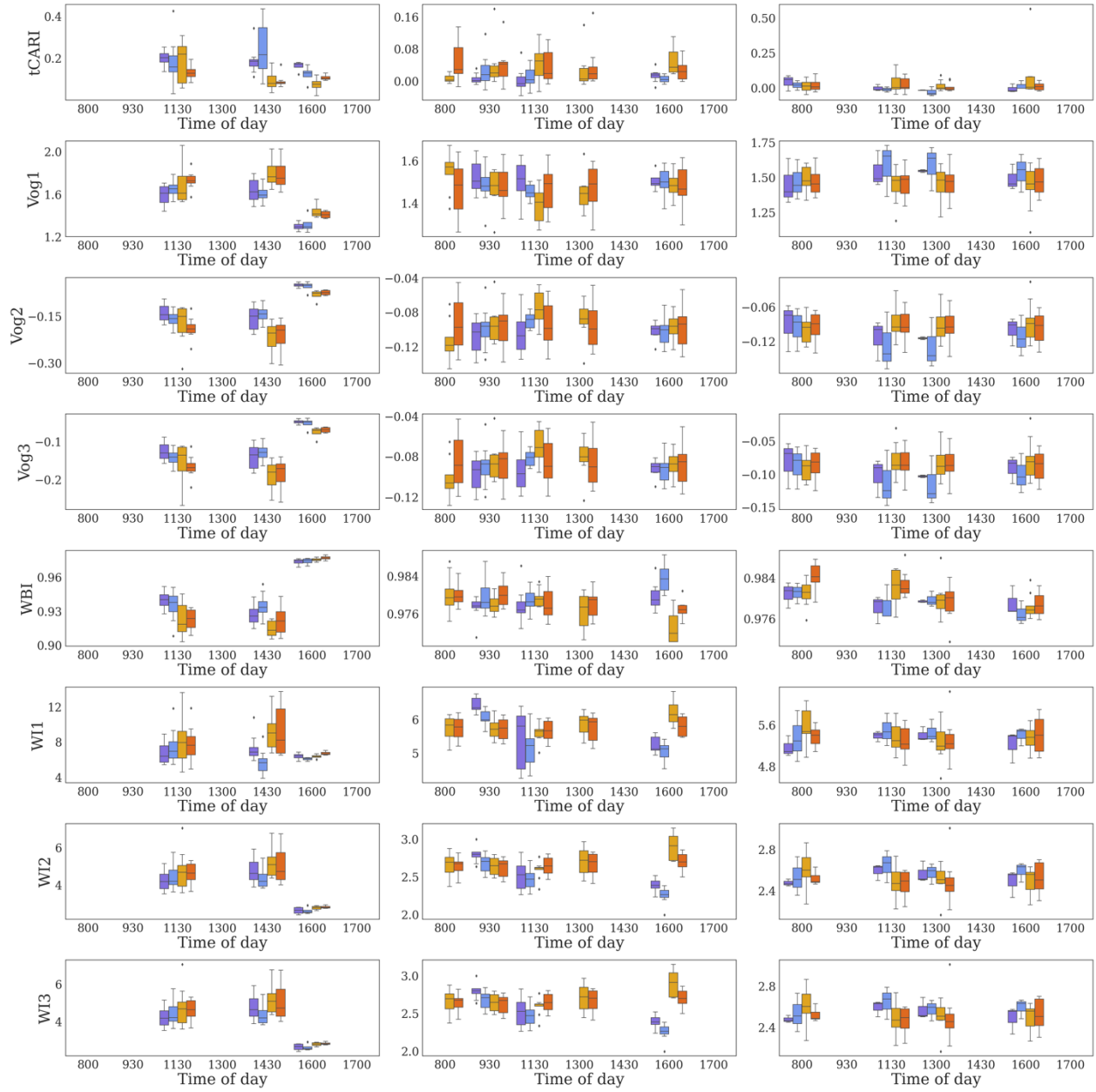
**Supplementary Figure 1 (cont'd).**



Supplementary Figure 1 (cont'd).

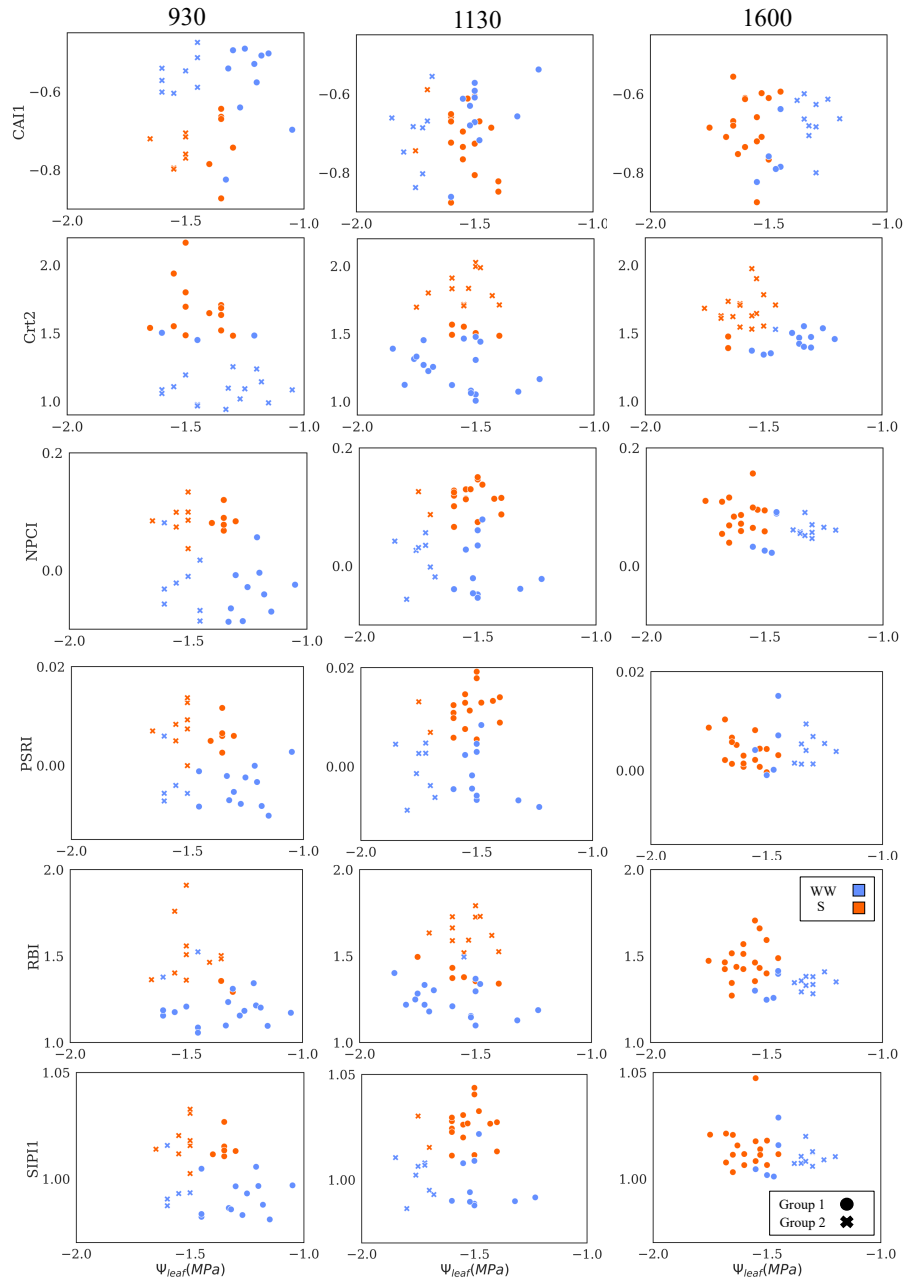


**Supplementary Figure 1 (cont'd).**

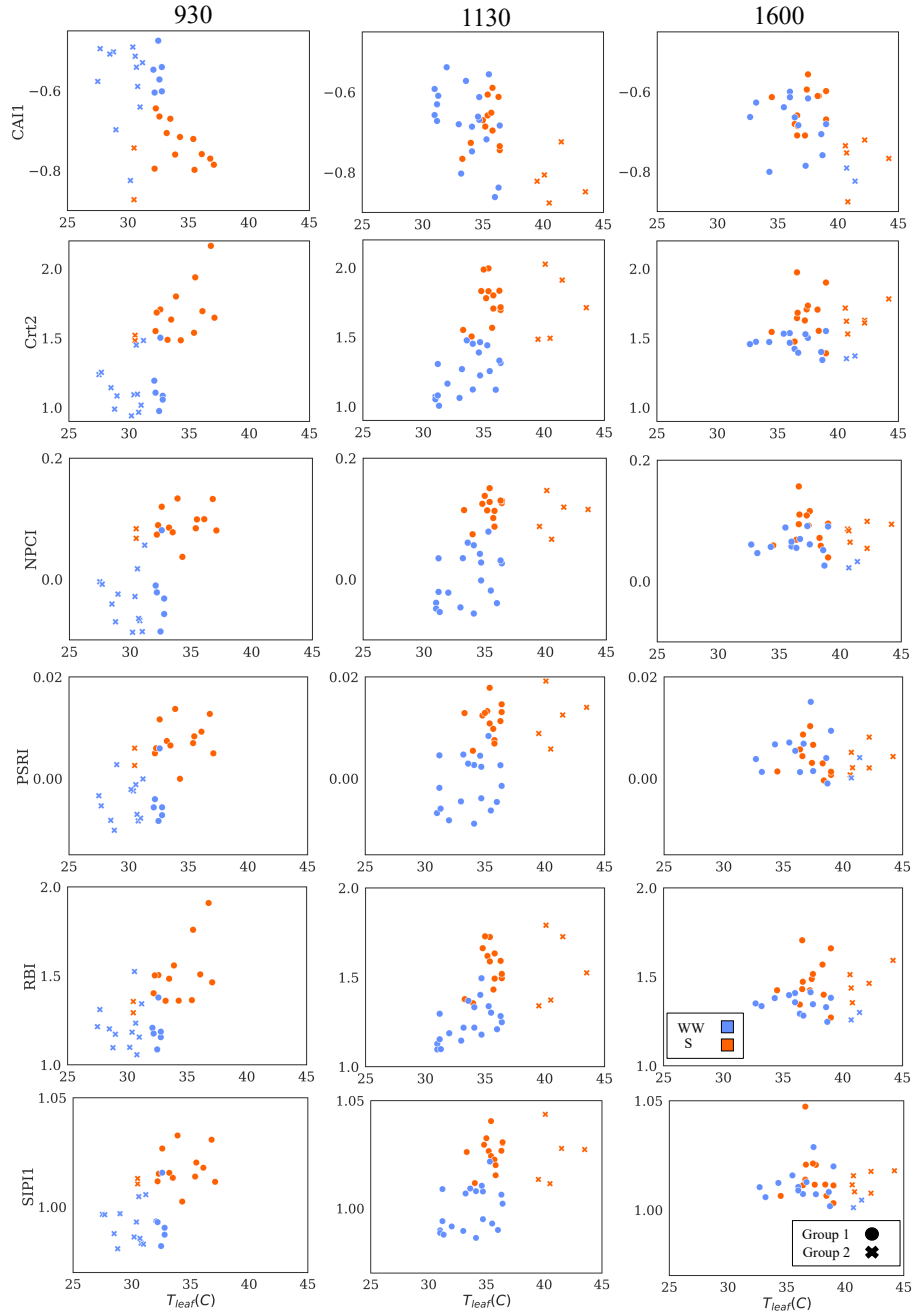


**Supplementary Figure 1 (cont'd).**

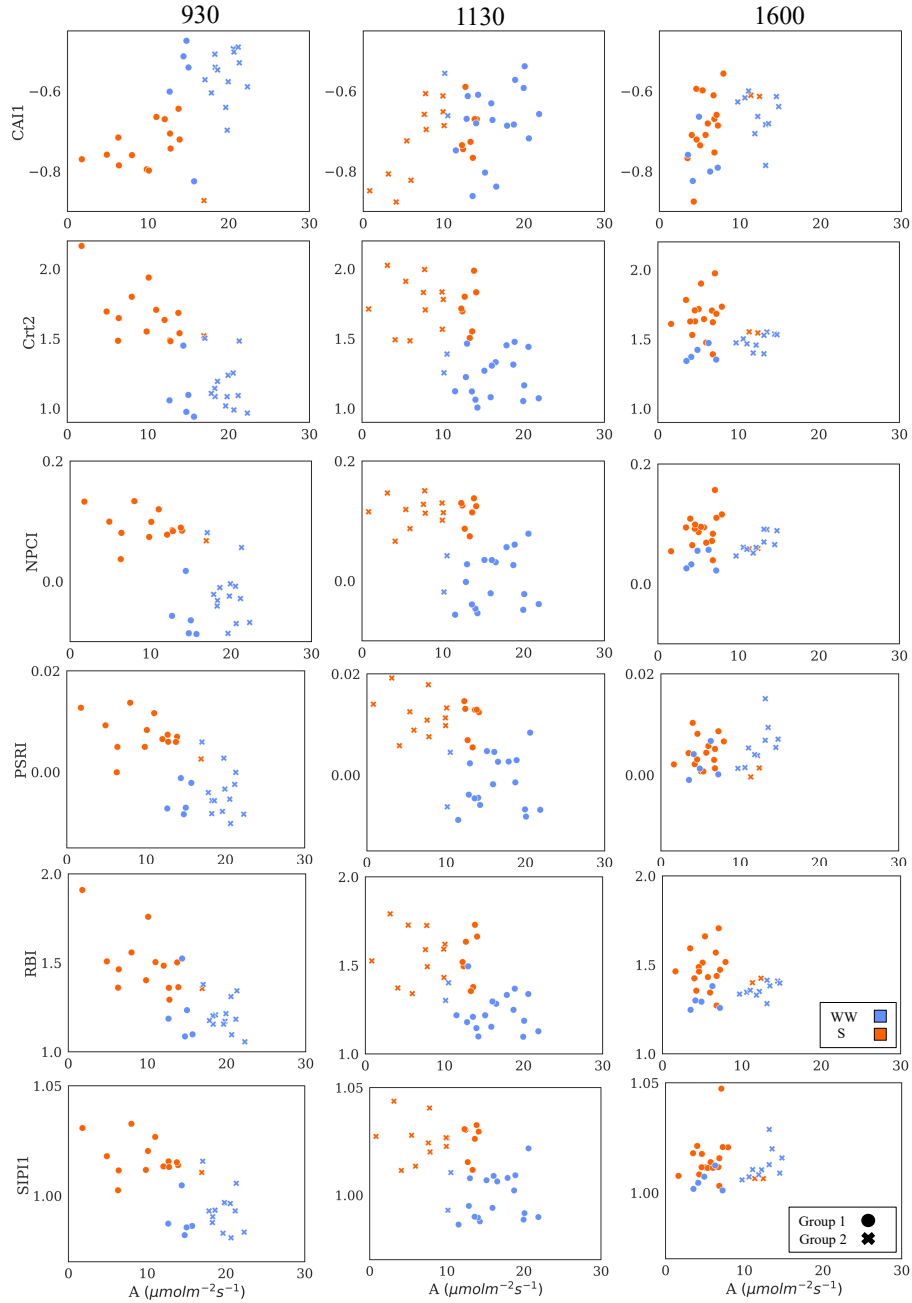




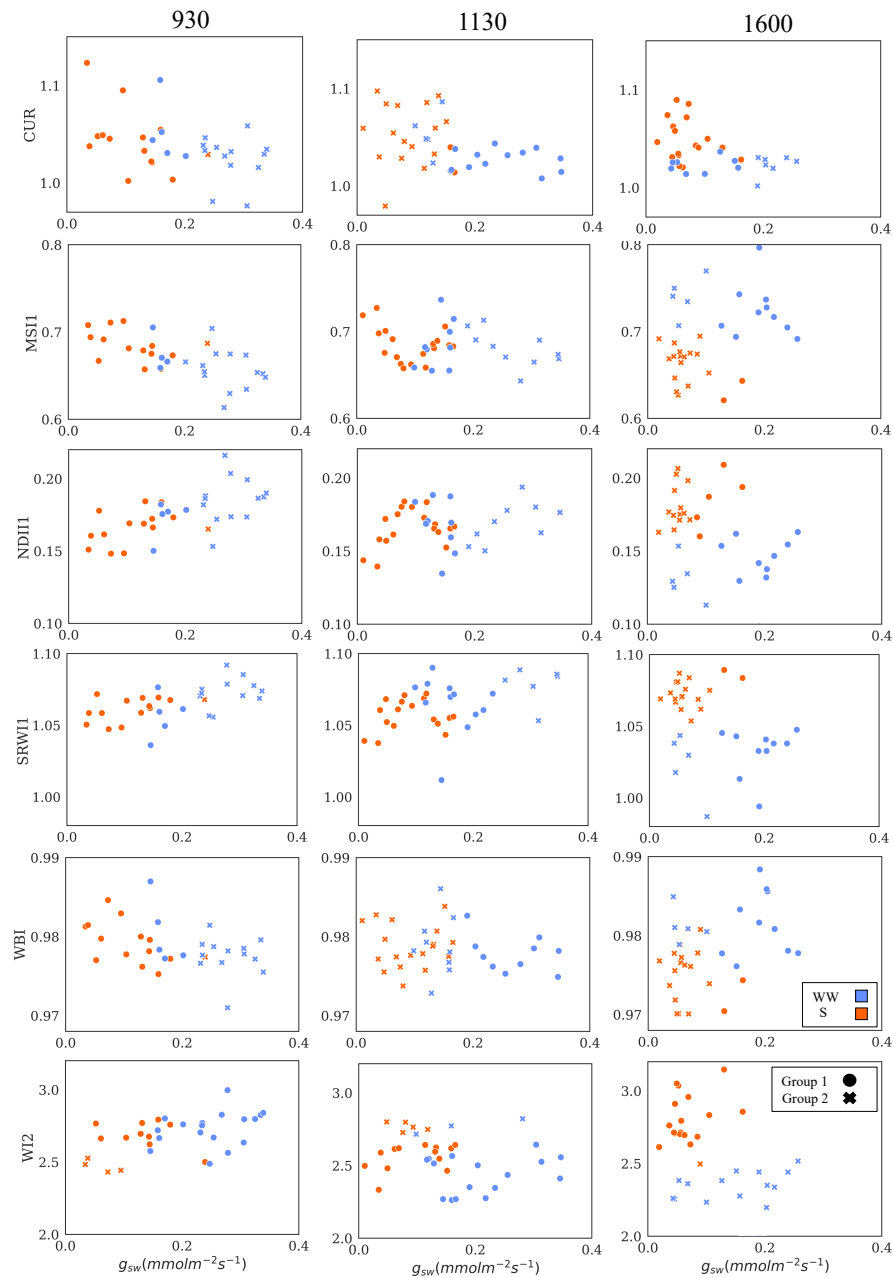
**Supplementary Figure 2.** Cluster results between selected hyperspectral vegetation indices (HVIs) and leaf water potential ( $\Psi_{\text{leaf}}$ ). Data collected from mildly and well-watered blocks were combined as well-watered (WW) blocks and stressed (S) block data were combined. Cluster results were evaluated using Birch (Balanced Iterative Reducing and Clustering using Hierarchies) clustering algorithm (threshold=0.01, n=2). Resulting groups ( $\bullet$ ,  $\times$ ) are assigned based on the clustering algorithm and have no relationship to treatment conditions.



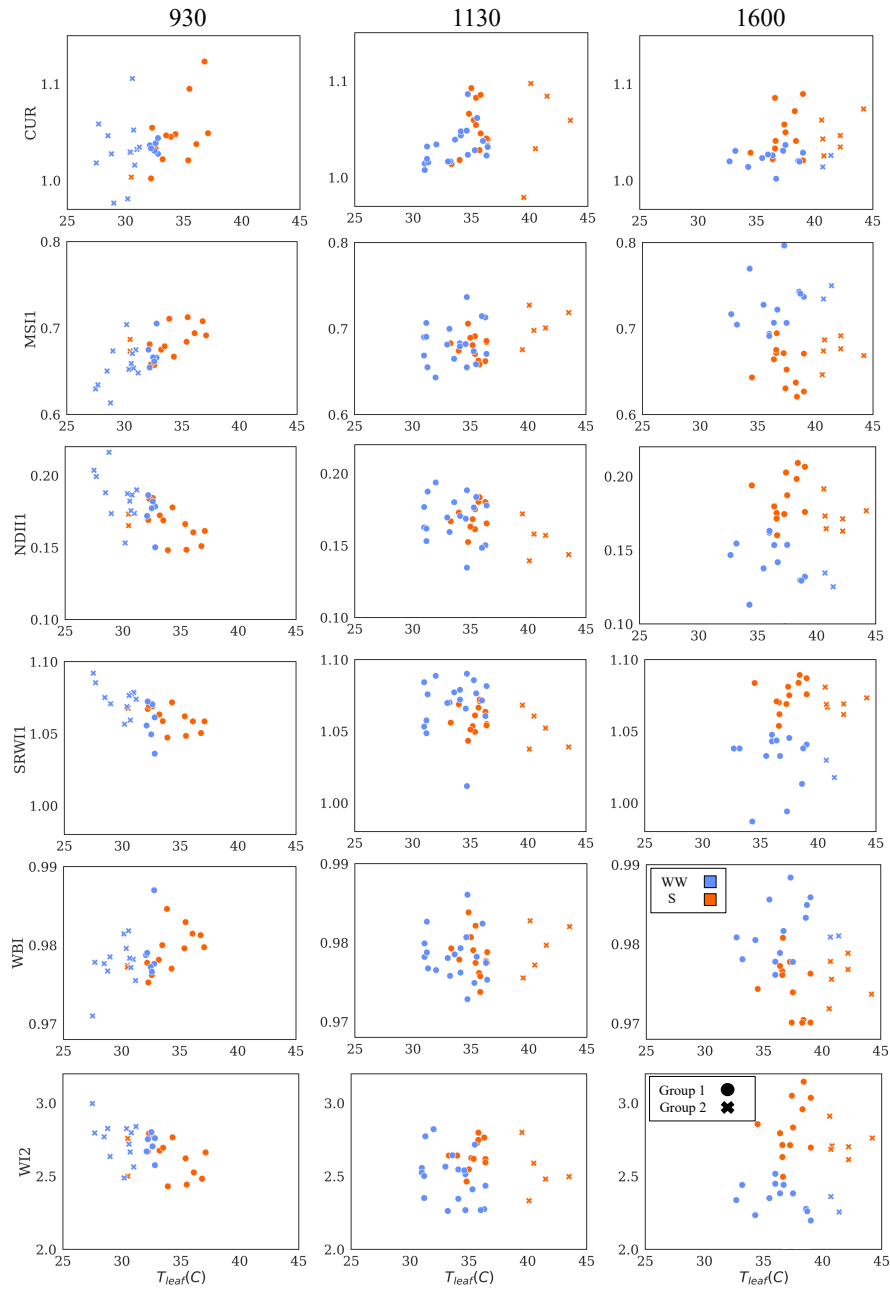
**Supplementary Figure 3.** Cluster results between selected hyperspectral vegetation indices (HVIs) and leaf temperature ( $T_{leaf}$ ). Data collected from mildly and well-watered blocks were combined as well-watered (WW) blocks and stressed (S) block data were combined. Cluster results ions were evaluated using Birch (Balanced Iterative Reducing and Clustering using Hierarchies) clustering algorithm (threshold=0.01, n=2). Resulting groups ( $\bullet$ ,  $\times$ ) are assigned based on the clustering algorithm and have no relationship to treatment conditions.



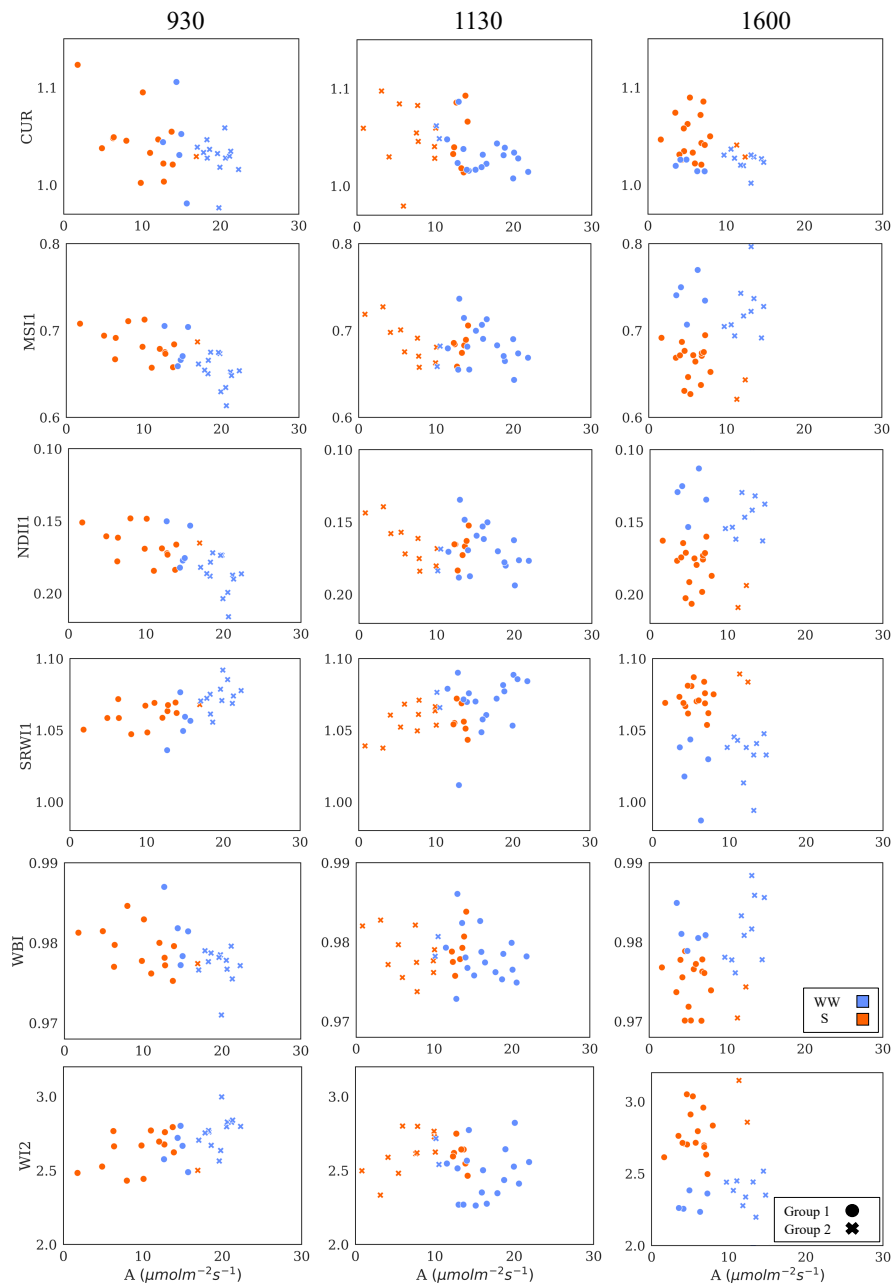
**Supplementary Figure 4.** Cluster results between selected hyperspectral vegetation indices (HVIs) and net assimilation (A). Data collected from mildly and well-watered blocks were combined as well-watered (WW) blocks and stressed (S) block data were combined. Cluster results were evaluated using Birch (Balanced Iterative Reducing and Clustering using Hierarchies) clustering algorithm (threshold=0.01, n=2). Resulting groups (●, ×) are assigned based on the clustering algorithm and have no relationship to treatment conditions.



**Supplementary Figure 5.** Cluster results between selected hyperspectral vegetation indices (HVIs) and stomatal conductance ( $g_{sw}$ ). Data collected from mildly and well-watered blocks were combined as well-watered (WW) blocks and stressed (S) block data were combined. Cluster results were evaluated using Birch (Balanced Iterative Reducing and Clustering using Hierarchies) clustering algorithm (threshold=0.01,  $n=2$ ). Resulting groups ( $\bullet$ ,  $\times$ ) are assigned based on the clustering algorithm and have no relationship to treatment conditions.



**Supplementary Figure 6.** Cluster results between selected hyperspectral vegetation indices (HVIs) and leaf temperature ( $T_{leaf}$ ). Data collected from mildly and well-watered blocks were combined as well-watered (WW) blocks and stressed (S) block data were combined. Cluster results were evaluated using Birch (Balanced Iterative Reducing and Clustering using Hierarchies) clustering algorithm (threshold=0.01, n=2). Resulting groups ( $\bullet$ ,  $\ast$ ) are assigned based on the clustering algorithm and have no relationship to treatment conditions.



**Supplementary Figure 7.** Cluster results between selected hyperspectral vegetation indices (HVIs) and net assimilation (A). Data collected from mildly and well-watered blocks were combined as well-watered (WW) blocks and stressed (S) block data were combined. Cluster results were evaluated using Birch (Balanced Iterative Reducing and Clustering using Hierarchies) clustering algorithm (threshold=0.01, n=2). Resulting groups (●, x) are assigned based on the clustering algorithm and have no relationship to treatment conditions.